Liquid Crystal Soft Actuators and Robots toward Mixed Reality

Chongyu Zhu, Yao Lu, Lixin Jiang, and Yanlei Yu*

Liquid crystals (LCs) are soft but smart materials that can adjust its chemical or physical properties in response to various external stimuli. Using these materials to construct soft actuators and robots, referred as LC actuators and robots, is expected to replace current machinery part, obtaining lighter and smaller equipment with adjustable and complex functions. Especially, combining these LC actuator and robots with existing virtual reality and augmented reality technologies will produce a new world of mixed reality (MR) with the visual, auditory, and somatosensory interaction. In this review, the recent work on responsive LC actuators and robots is introduced, emphasizing on their potentials in haptic use. By discussing their programmable control via suitable stimuli, the LC actuators and robots are summarized for mechanical outputs, environmental mimic, and fine-tuning of surface texture and roughness. It is anticipated that the continuous development on LC actuators and robots will accelerate the MR technology toward practical application.

1. Introduction

With the aid of computer-controlled sensors, actuators, controllers, displays, etc., new technologies such as virtual reality (VR)[1,2] and augmented reality (AR)[3,4] have brought new sensory experience to people. For example, introducing visual and auditory information by computer software through wearable devices, VR presents users an artificial world that they can interact and accept it like a real one.[5–7] AR, on the other hand, integrates digital data into actual environment through recognizable marker (i.e., barcode/Quick Response Code).[8–10] Although the first VR prototype appeared only a few decades ago, these techniques have been widely used in medical,[11] military,[12] aerospace,[13] and other fields.[14,15] Recently, a new concept of combining VR and AR has been proposed, namely mixed reality (MR) or hybrid reality.[16] Compared to VR and AR, MR involves the interaction among human, computer, and environment, which is expected to provide more immersive and "real" experience.[17,18]

To join the physical world with the digital world requires not only the optimization of the current complicated calculation methods with suitable software, but also the continuous development on hardware.[19] In addition to the visual and auditory information that can be supplied by current VR and AR systems, introducing actuators and robotic systems into MR systems will offer somatosensory interaction to users,[20] further promoting their practical applications in remote-control surgery,[21] bionic prosthesis,[22] precision aircraft control,[16] etc. Even though various devices (i.e., VR cabin,[23] helmet,[24] gloves,[25] etc.) have been created to collect the motions of users, they are unable to offer haptic feedback with sufficient interaction among human, computer, and environment. Moreover, the bulky devices along with complex external circuits hinder the degree of freedom to users, burdening their operations.

Recent years have witnessed the development of smart materials, or stimuli-responsive materials, which can sense subtle variation in the environment and provide intrinsic property changes including shape,[26,27] color,[28] conductivity,[29] light transmittance,[30] etc. Exploring these materials to construct "smart" MR equipment will reduce the size and the weight of current devices as well to simplify the programming design to current control systems, offering better user experience. To match the haptic use in MR application, the smart materials should meet the following requirements. i) The ideal material should provide controllable and rapid deformation in response to external stimuli to output programmable and real-time mechanical signals; ii) soft and biocompatible textile is required to ensure a fit and comfortable compliment, avoiding physical or chemical damage to users; and iii) non-contact stimuli are preferred to omit additional wired connections.

Among all smart materials, liquid crystal polymers (LCPs) are promising candidates to construct haptic feedback systems for MR applications. Incorporating the liquid crystal (LC) mesogens into the polymer backbones or side chains, LCPs inherit the advantages of both LC and polymers, possessing flexible, low density, excellent mechanical properties, and quick response.[31–33] By simply adjusting the orientation of LC through various fabrication techniques, these LCPs can perform different deformation modes, such as contraction and expansion,[34–36] topographical deformation,[37–39] bending,[40–42] twisting, and rolling,[43–45] etc. Combining these deformation

Dr. C. Zhu, Y. Lu, L. Jiang, Prof. Y. Yu
Department of Materials Science and State Key Laboratory of Molecular
Engineering of Polymers
Fudan University
220 Handan Road, Shanghai 200433, China
E-mail: ylyu@fudan.edu.cn

The ORCID identification number(s) for the author(s) of this article
can be found under https://doi.org/10.1002/adfm.202009835.

ADVANCED
SCIENCE NEWS
www.advancedsciencenews.com

ADVANCED
FUNCTIONAL
MATERIALS
www.afm-journal.de

modes results in diverse soft actuators and robots, providing a toolbox for constructing MR systems with somatosensory interaction.[46–50] In comparison to rigid motors or other conventional machinery actuators, actuators and robots made of LCPs (LC actuators and robots) are smaller, lighter and "smarter", which can provide better and smoother somatosensory interaction and realize more complex functions.[51–57] In addition to performing rapid and delicate deformations/motions under the control of computer programs,[58–60] these "smart" actuators and robots can also interact directly with users when external stimuli changes, enhancing the real-time haptic feedback.

In this review, we summarize the current soft LC actuators and robots with potential in MR applications. We start with the design principle of LCPs and their actuation mechanisms by different stimuli, emphasizing on their programmable control by electricity and light. Categorized by their functions, we then highlight the LC soft actuators with different mechanical output modes. By discussing the importance of LCPs, we outline various bio-inspired soft robots mimicking the motions and functions of nature creatures. The LC surfaces with adjustable morphologies and topologies are also covered as they allow a fine-tuning of tactile feeling. Although the current functions of the mentioned LC actuators and robots remain relatively simple, we hope this review will be useful to guide the design of new LC materials as well as new LC actuators and robots that will be applied in MR applications.

2. Programmable Control of LCP Deformations for MR applications

Since the first VR device was born in 1962, LC materials have been supporting the development of VR/AR technology. Owing to the dielectric anisotropy and birefringence property of LC small molecules, they are widely used in VR/AR display to offer realistic visual experience.[61,62] For instance, electric-responsive nematic LC small molecules are important materials in the output devices such as VR goggles.[63] Through electro-optical effect by external electric fields, the LC mesogens undergo reorientation or phase transition to produce different patterns by refracting or shielding light. Although various LC small molecules have been developed and commercialized, it is still essential to seek new LC small molecules for VR/AR display with high-resolution (for example, "retina display" resolution, that is, more than 300 pixels per inch[64,65]), rapid screen reflash rate (more than 60 frames per second) and 360° panoramic imaging.

The investigation on responsive LCPs has also received increasing attention over the last decades;[66,67] however, their potential in VR/AR/MR application was rarely mentioned until the concept of haptic display was proposed. The deformation of LCPs upon external stimuli is one of the most important parameters for their potential in haptic use toward MR application, which is greatly relied on the orientation change of LC mesogens.[68–70] Therefore, choosing suitable stimuli to change the order parameter of LCPs is crucial for the programmable control of LCP deformation toward diverse functions.[33,71]

2.1. Electro-Induced LCP Deformation

Electrical signals such as current and voltage are easy to be programmed by computers, giving command to the current VR mechanical output devices. Adapting electro-active LCPs into current systems may reduce the device sizes and provide more precise control[72] with bio-friendly somatosensory interaction.

As mentioned earlier, LC small molecules are dielectric anisotropic. In 1962, Richard Williams first observed a regular pattern formed by the reorientation of nematic LC in an external electric field, which opens the application of LC display.[73] Although the re-alignment of LC small molecules induced by electricity will only produce changes at the molecular level, it was discovered that the order parameters of LC in LCPs can also be re-arranged in response to electric field and the LC reorientation will be amplified through the polymer network and induce macroscopic deformation of LCPs.[74] For example, using a flexible and transparent ferroelectric LCP with a polysiloxane backbone, Kremer et al. demonstrated the electric-induced LC reorientation in LCP films at an alternating current (AC) electric field of 1.5 kV mm^{-1}.[75] Induced by an AC electric field, the LCP underwent phase transition between S_A^* phase and S_C^* phase (**Figure 1**a), varying the layer thickness (Figure 1b). Since only a slight change of LC order degree was achieved by this mechanism, the shape variations were at nanometer level. To match the deformation, the thickness of LCP films should be less than 1 μm. Thus, this deformation control mechanism is often used to construct micro/nano-scaled machines.

Another approach to fabricated an electro-deformable LCP is to coat or embed resistance materials such as carbon black, copper wires, silver inks onto/into a thermoresponsive LCP.[76–78] Through electrothermal effect, or the Joule effect, the resistance materials will convert electric power to thermal energy, heating up the LCP above its LC-isotropic phase transition temperature (T_i) so that the LC mesogens turn from an ordered state to disordered state, resulting in a macroscopic shape deformation of LCP.[79] For example, Cai et al. fabricated an electrothermal responsive LCP tubular actuator by the incorporation of serpentine heating wires.[80] When an electrical potential was applied onto unilateral heating wires, the LCP went through LC-isotropic phase transition by the Joule effect and contracted asymmetrically to drive the tubular actuator to bend to a specific direction (Figure 1c). They then assembled three tubular actuators into a soft gripper, and controlled it to grab and lift a vial or unscrew the vial lid by selectively Joule heating each tubular actuator (Figure 1d).

However, the rigid fillers/additives may alter the mechanical properties of the original LCPs, hindering their deformations. To overcome this limitation, Majidi et al. reported an electroresponsive LCP composite that was composed of a thermoresponsive LCP ($T_i \approx 65$ °C) embedded with 50 vol% liquid metal (LM) inclusions.[81] Possessing high electrical and thermal conductivity, this LCP composite produced quick and reversible macroscopic shape variation at a rate faster than 2 Hz by Joule heating. With the aid of this LCP composite, they then fabricated a transducer to sense touch, which may be used as haptic soft sensors in MR applications. Yet, the high LM content remains a barrier to its practical application. Therefore, the same group[82] developed alternative approach
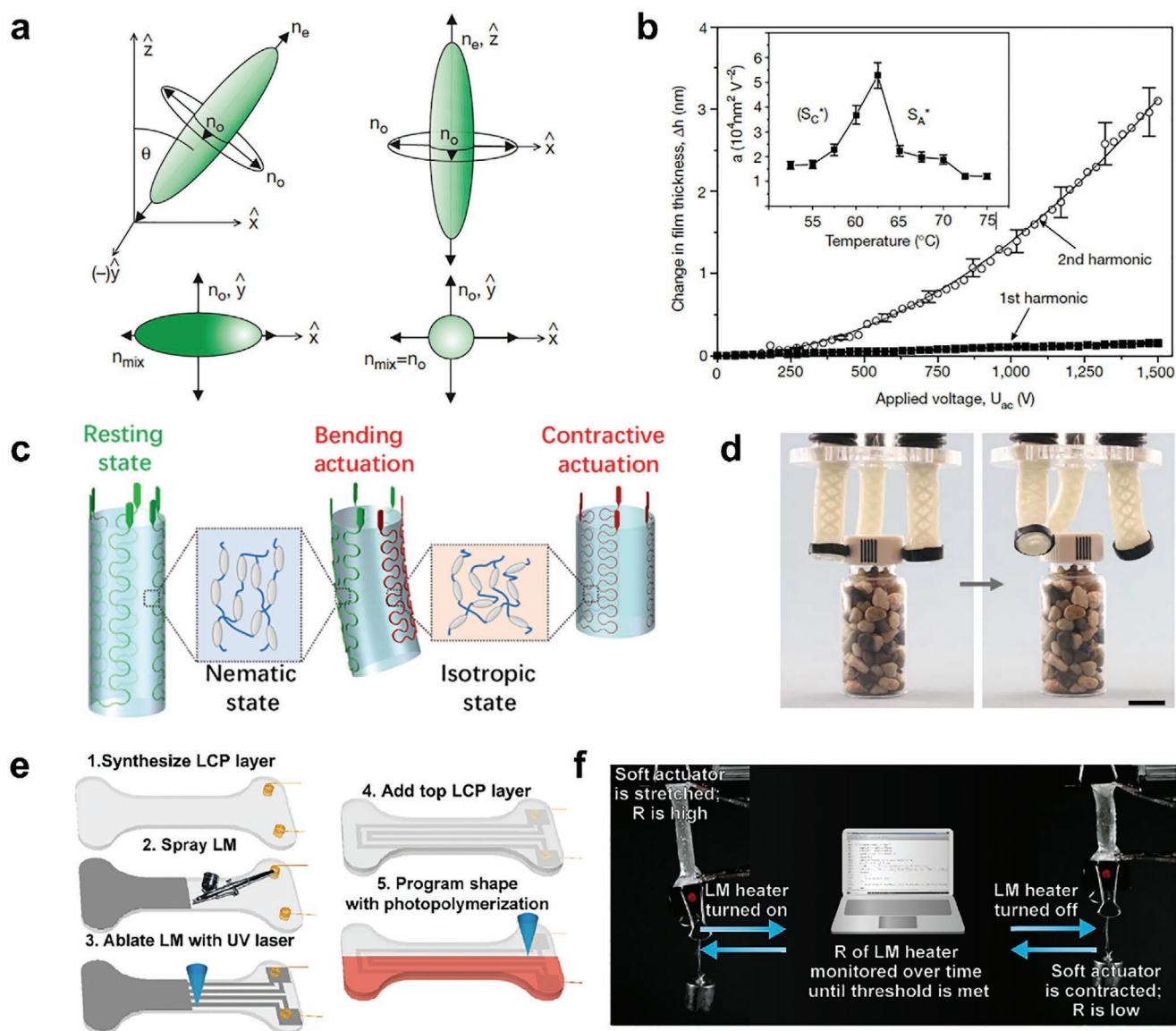
Figure 1. a) Schematic showing optical axes of LC mesogens in tilted (biaxial) state and non-tilted state when the AC electric field was on/off. b) The thickness change of LCP film with the increase of applied voltage. Reproduced with permission.[75] Copyright 2001, Springer Nature. c) A schematic diagram showing the working principle of the LCP tubular actuator. The asymmetric bending actuation and uniform contraction of the tubular actuator are achieved by applying a potential to one or all of the heating wires (highlighted in red). d) Unscrewing the vial cap by the soft gripper made from three LCP tubular actuators. Scale bar, 1 cm. Reproduced with permission.[80] Copyright 2019, American Association for the Advancement of Science. e) Step-by-step schematic describing fabrication of UV laser-ablated liquid metal (LM) Joule heaters atop LCPs. f) Programmable shape deformations of LCP/LM composite by controlling the LM heater on/off. Reproduced with permission.[82] Copyright 2021, IOP Publishing.

to fabricate LCP/LM composite. LM was first sprayed between two LCP layers and patterned into the circuit by ultraviolet (UV) laser ablation (Figure 1e). Encapsulated by two LCP layers, the LM circuit stayed intact and electrically conductive even when the LCP deformed, avoiding electromigration failure. Through this LCP composite, programmable shape deformations were realized through the Joule effect (Figure 1f), outputting a specific work density up to 9.2 J kg^{-1}. Since the resistance of this composite was correlated to the changes in strain and the surrounding environmental temperature, it can be used as a force and temperature sensor for MR applications.

2.2. Photo-Induced LCP Deformation

Similar to electricity, the parameters of light, such as wavelength and intensity, are also tunable and programmable.[40,46,83] More importantly, light enables the remote and precise control, which is difficult to be realized by other stimuli.[84,85] Fabricating photoresponsive LCPs into soft robots and sensors is likely to be used in "smart" MR devices with remote control, which is favored for multi-user applications. A straightforward method to obtain photoresponsive LCPs is the incorporation of photothermal dyes (i.e., azobenzene derivatives,[86,87] organic or organometallic dyes[71,88]) or agents (such as gold

**ADVANCED
SCIENCE NEWS**
www.advancedsciencenews.com

**ADVANCED
FUNCTIONAL
MATERIALS**
www.afm-journal.de

nanoparticles,[54,89] carbon nanotubes[90,91] and polydopamine coatings[92,93]) into thermoresponsive LCPs. Through photothermal effect, these LCPs will be heated up and go through LC-isotropic phase transition just like other thermoresponsive LCPs, producing macroscopic deformations (**Figure 2**a).[94] For instance, with the aid of a new photoreduction method to spatially incorporate gold nanoparticles into a thermoresponsive monodomain nematic LCP, DeSimone, Jin, and Hayward et al. prepared photoresponsive LCP composite films with tunable patterns.[95] Upon 200 mW cm^{-2} of 530 nm light, LCP was heated via photothermal effect and expanded asymmetrically to perform complex actuation. This approach requires no need of additional complex control devices or photomasks for photoresponsive LCP actuation, which provides an alternative design for MR haptic devices.

Alternatively, photo-induced deformation can occur without generating heat in some LCPs containing photochromic LC mesogens, such as diarylethenes,[96,97] hydrazones,[98,99] azobenzene,[100,101] etc. When exposed to suitable light, these mesogens undergo molecular geometric change (typically *trans–cis* isomerization), which disrupts the orientation of LC mesogens, leading to photochemical LC phase transition (Figure 2b). Compared with deformations driven by photothermal-induced LC phase transition, photochemical LC phase transition allows a non-thermal control of LCP deformations, which offers somatosensory interaction at a milder condition. Yet, the *trans–cis* isomerization of these photochromic molecules is often achieved under UV light, which is not always favored for human interactions. By developing an azobenzene derivative with a long-conjugated structure as the photoresponsive LC mesogen (Figure 2c), Yu et al. realized the bending and unbending of LCPs driven only by visible light.[102] By combining this visible light-responsive LCP film with a polyethylene film, they constructed a LC soft robot consist of an arm, wrist, and hand (Figure 2d). Through light manipulation, this robot managed to pick, lift, move, and place objects 10 times of its own weight without additional gears or motors (Figure 2e), demonstrating its potential in micromechanical systems. With a more bio-friendly stimulus, these photoresponsive LCPs will accelerate the development of remote-control MR devices.

As for azobenzene-containing LCPs (azo-LCPs), their deformations can also be triggered by photoreorientation (also known as the Weigert effect).[103–105] When shined by certain light (typically blue light), the azobenzene molecules in azo-LCPs absorb the light energy and undergo repeated *trans–cis–trans* isomerization cycle, changing their orientation to the position where they are unable to absorb more light energy. As a result, the azobenzene units will be re-aligned either perpendicular (when polarized light is used) or parallel (when non-polarized light is used) to the direction of incident light (Figure 2f). Different from photochemical phase transition abovementioned, most azobenzene molecules in azo-LCPs are still in the stable *trans* state when photoreorientation occurs. For example, White et al. reported the bending deformation of polydomain azo-LCPs in a glassy state under the linear polarized blue-green (442–514 nm) irradiation (Figure 2g).[106] The continuous *trans–cis–trans* isomerization of azobenzene under blue–green irradiation resulted in the asymmetric deformation and macroscopic

bending while the film remained in a glassy state. Since the rearrangement of LC was controlled by the polarization direction of the light, the bending direction of the azo-LCP film was controllable by a single light source (Figure 2h). This photo-control mechanism may help to develop MR devices with good mechanical property and easier control.

3. LC Actuators for Mechanical Output

Components for mechanical output are the main part of haptic devices in MR application. Compared with conventional actuators that are often with predetermined single performance once fabricated, some LC actuators are reprogrammable so that they can produce different forms of mechanical output as requested. Moreover, most current actuators that are powered by electricity, while LC actuators have a wide choice of power source and can recognize signals from many stimuli such as heat,[34] electricity,[33] light,[44,45] and their combination.[32] In this section, we will introduce the LC actuators with different mechanical output modes.

3.1. Motors

Motors are commonly used to generate continuous motions, which is essential for MR haptic use. In comparison to machinery motors, the motors prepared by LCPs (LC motors) are much lighter and with smaller sizes so that they are likely to be applied in wearable applications. Among all stimuli, light is often used to construct such LC motors. For example, Ikeda et al. constructed a photo-driven motor consisted of two bearings and a photoresponsive laminated belt (**Figure 3**a).[107] The belt was composed of a well-aligned azobenzene containing LCP (Figure 3b) and a commercially available PE film. When UV light (366 nm, 200 mW cm^{-2}) and visible light (>500 nm, 120 mW cm^{-2}) were irradiated at the left and right bearings, the belt rolled counterclockwise (Figure 3b, c). During this process, the azobenzene mesogens at UV illuminated part underwent *trans–cis* isomerization, disturbing LC orientation and causing the contraction of the film to generate contraction force locally. On the other hand, azobenzene mesogens at visible illumination underwent *cis–trans* isomerization so that LC orientation was recovered and the film turned back to its original state, producing a local expansion force. Since the positions of the two light sources were fixed, the rotation driven by photoirradiation would continuously deliver recovered part for UV irradiation and the UV illuminated part to be exposed by visible light (Figure 3c), giving a battery-free motor system for continuous mechanical output. This work offers a new approach to supply power, which may be useful for battery-free MR devices.

Electroresponsive LCPs can convert electric power into mechanical output. Yang et al. presented a bilayer electroresponsive cylindrical actuator that rolled along a conductive track at a rate of 1.6 mm s^{-1} when applying a 50 V direct current as the power source.[108] The cylindrical actuator consisted of a monodomain nematic LCP (**Figure 4**a) coated with several U-shaped carbon black conductive regions. Once a U-shaped
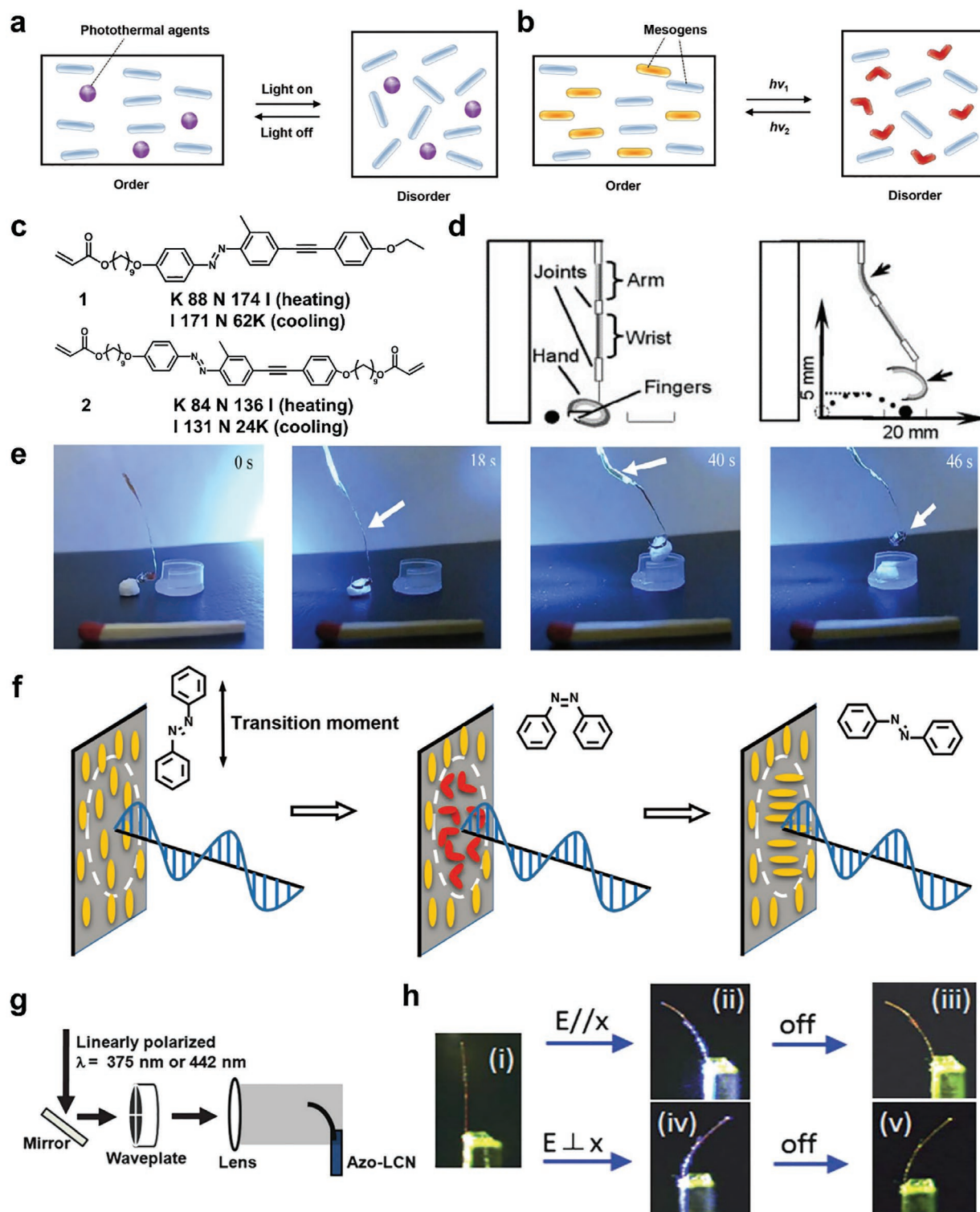
Figure 2. a) Photothermal-induced and b) photochemical-induced order-disorder phase transition of LCPs. Reproduced with permission.[94] Copyright 2019, Wiley-VCH. c) Chemical structures of azobenzene derivatives (monomer 1 and crosslinker 2) with a long-conjugated structure for the synthesis of visible light-responsive LC soft robot. K, crystal; N, nematic; I, isotropic. d) Schematics showing the assembly and control of the LC soft robot for object transport. e) Photographs of the LC soft robot to pick, lift, move, and place an object to a nearby container in response to blue light. The illuminated parts were labeled by white arrows. Reproduced with permission.[102] Copyright 2012, Royal Society of Chemistry. f) Photoreorientation of azobenzene containing LCPs by linearly polarized light. Reproduced with permission.[50] Copyright 2019, Wiley-VCH. g) Optical setup with linearly polarized light for light-induced bending. h) Polarization-controlled forward and reverse bending of the LCP film by a single light source. Reproduced with permission.[106] Copyright 2012, Royal Society of Chemistry.
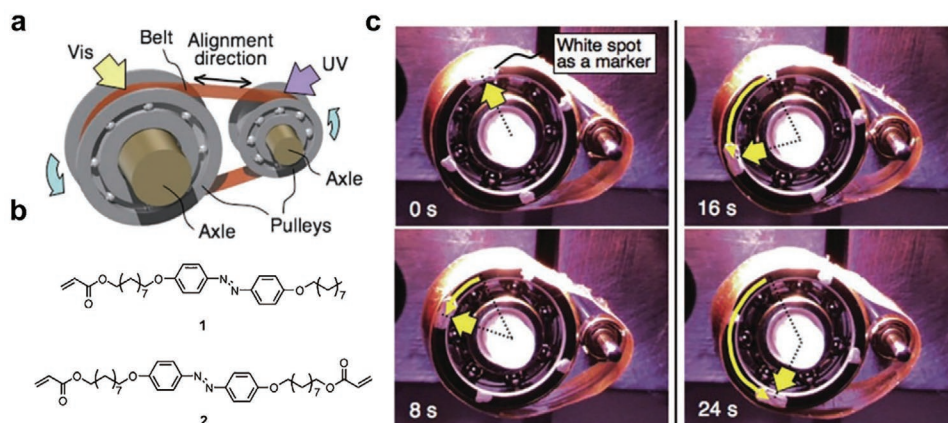
Figure 3. a) Schematic of the photo-driven motor consisting two bearings and a photoresponsive laminated belt. b) Chemical structures of the LC monomer 1 and LC diacrylate 2 used for constructing the photo-driven motor. c) Images to show the motor under irradiation. Reproduced with permission.[107] Copyright 2012, Wiley-VCH.

carbon black region contacted the conductive track, it formed a circuit that heated the LCP layer through the Joule effect, thereby disrupting the nematic phase of the LCP. The LCP layer was then contracted, deforming the cylindrical structure and changing the gravity center of the actuator (Figure 4b). As the actuator moved forward, the U-shaped carbon black region disconnected and Joule heating stopped so that the contracted area of the LCP recovered to its original state. Meanwhile, the next U-shaped carbon black region formed a new circuit in contact with the conductive track, heating and deforming the new area of LCP. Therefore, the cylindrical actuator was able to roll forward continuously (Figure 4c).

Besides belt-like actuators, actuators with other forms can also output mechanical energy. For example, Cai et al. composited a cylindrical monodomain thermoresponsive LCP with carbon nanotubes (CNTs) to obtain a rod-like LC robot (70.0 mm length and 2.6 mm diameter) and demonstrated its motion powered by light or heat. In the case of light-driven motion, the rod-like robot was heated by the photothermal effect of CNTs upon illumination of white light with a power density of 300 mW cm^{-2}.[109] When the temperature reached above the T_i of LCP, the rod surface contracted asymmetrically, rolling clockwise or counterclockwise depending on the initial curvature of the rod formed during fabrication (Figure 4d). Moreover, this LC rod-like robot can be assembled into more complex forms, that is, an underwater vehicle (Figure 4e,f), providing diverse modes of mechanical output.
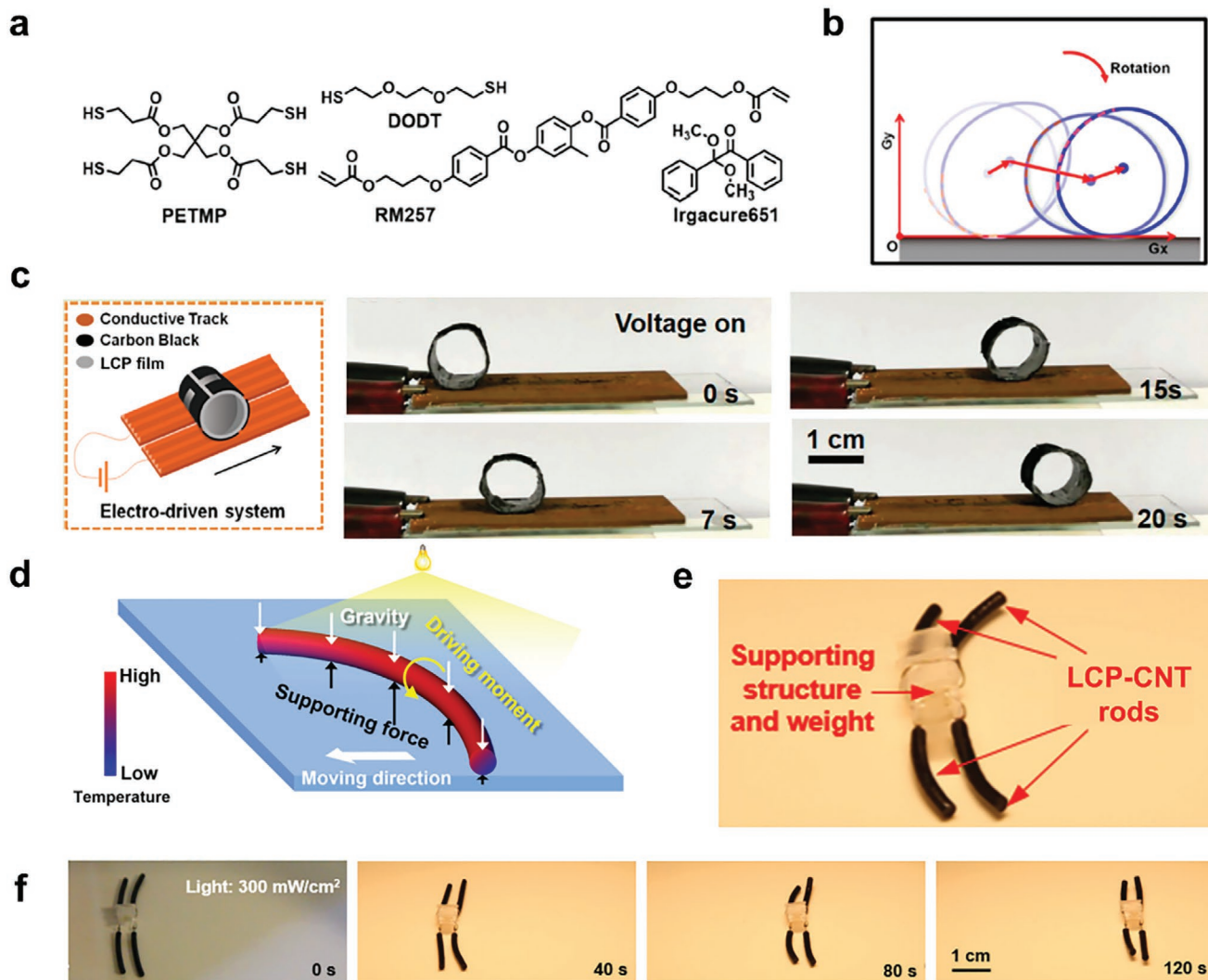
Inspired by piezoelectric ultrasonic motors, Wasylczyk et al. fabricated flat ring-like micromotors using azo-LCPs with the two surfaces possessing azimuthal–azimuthal (A/A-motor) or azimuthal–radial LC orientation (A/R-motor).[110] When a rotated 532 nm laser beam with a power of 5.0 W irradiated locally on the position of the micromotors, the local heating of the azo-LCPs induced by photothermal effect caused a reversible nematic-isotropic phase transition, producing 3D deformations. As a result, the A/A-motor deformed into a conical structure, while the A/R-motor exhibited a saddle topology. Followed the scanning direction of laser beam, both motors produced a rotary motion. Although A/R-motor rotated much faster (around ten times) than the A/A-motor owing to a better

coupled friction generated between the conical structure and the stator, the A/A-motor offered a more stable and regular output, which may be useful to drive MR haptic devices in the future.

3.2. Oscillators

Oscillators are another important source of continuous mechanical output, which provide reciprocating oscillation that has been widely used in the mechanical field. Compared with macro-scaled oscillators, microactuators with high frequency oscillation are more likely to be applied in MR microdevices, such as micro-aircrafts,[111] micro valves, or other micromechanical devices.

In 2008, Bunning et al. first reported the high-frequency oscillation of a LC cantilever by photoresponsvie monodomain azo-LCPs, converting the light energy into oscillated mechanical output.[112] The nematic azo-LCPs were prepared by the thermal copolymerization of two azobenzene LC monomers in LC cells. As showing in **Figure 5**a, applying a polarized multiwavelength (457, 488, and 514 nm) argon-ion (Ar$^+$) laser source (0.8 W cm^{-2}), they realized the oscillation of the LC cantilever with a displacement angle larger than 170° at a frequency of nearly 30 Hz. During illumination, the azobenzene units on the illuminated side underwent *trans–cis–trans* photoreorientation by the Weigert effect and rotated to the perpendicular position to the light director. Thus, the illuminated side contracted and bent the LC cantilever, so that the unilluminated side was exposed to the laser beam (Figure 5b). Next, the newly exposed side shrunk under the laser irradiation while the unexposed side was recovered by the entropy restoring force from polymer network coupled with the rapid reorientation of the azobenzene units. Therefore, the LC cantilever bent toward the opposite direction, generating oscillation continuously (Figure 5c). Adapting a similar strategy, they then optimized their system and demonstrated the oscillation of a LC cantilever with enhanced frequency and displacement angle under unpolarized light (focused sunlight) systems.[113] By simplifying the stimulus source, this work

**ADVANCED
SCIENCE NEWS**
www.advancedsciencenews.com

**ADVANCED
FUNCTIONAL
MATERIALS**
www.afm-journal.de

Figure 4. a) Chemical structures of the LC acrylate monomer (RM257), the cross-linker (PETMP), and the photoinitiator (Irgacure651) used for constructing cylindrical actuator. b) Schematic illustrating the gravity center shifting of the cylindrical actuator. c) Scheme and images of electro-driven rolling of the cylindrical actuator. Reproduced with permission.[108] Copyright 2020, American Chemical Society. d) Schematic showing the light-driven rolling of LCP-CNT composite rod upon irradiation of white light from the top. The LCP-CNT composite rod has the tendency of bending its two ends up due to thermal gradient along the thickness of the rod generated by the photothermal effect of CNTs. As a result, the supporting force provided by the surface gets concentrated to the middle part of the rod, and the moment generated by the supporting force and gravity drives the rod rolls to its concave direction. e) Structures of a vehicle composed of LCP-CNT rods and supporting structure and weight. f) Underwater motions of a vehicle driven by white light. Reproduce with permission.[109] Copyright 2018, American Chemical Society.

provides a power source for sustainable outdoor use toward MR applications.

In addition to 2D oscillation, 3D motion of a LC cantilever has also been realized. In 2012, White et al.[114] reported flexural-torsional response of LC oscillators. By cutting from a high modulus nematic LCP film at different directions, they obtained LC cantilevers with different mesogen orientations. Thus, various oscillation modes were presented upon illumination of linearly polarized 442 nm light (Figure 5d). Through this design, they realized a flexure-torsion simulation of insect's 3D flapping motion (including bending, twisting, and sweeping) (Figure 5e), showing the facile preparation of LC oscillators with higher oscillation frequency, larger vibration amplitude, and tunable oscillation modes.

The abovementioned cases require special designed azobenzene LC molecules or a specific light source, hindering the mass production of devices with reliable performance. In 2016, Meijer and Broer et al. developed a general method to manufacture self-sustained oscillators using commercially available materials (Figure 5f), further reducing costs and extending their service life.[115] By introducing conventional photostabilizers into the splay-aligned LCP made from commercial reactive mesogens (Figure 5g), they fabricated LC oscillators with different responding light stimulation, ranging from UV light, sunlight to near-infrared (NIR) light. Moreover, the oscillation frequency and amplitude of these LC oscillators can be customized, giving ideal candidates for oscillating haptic use in MR applications.
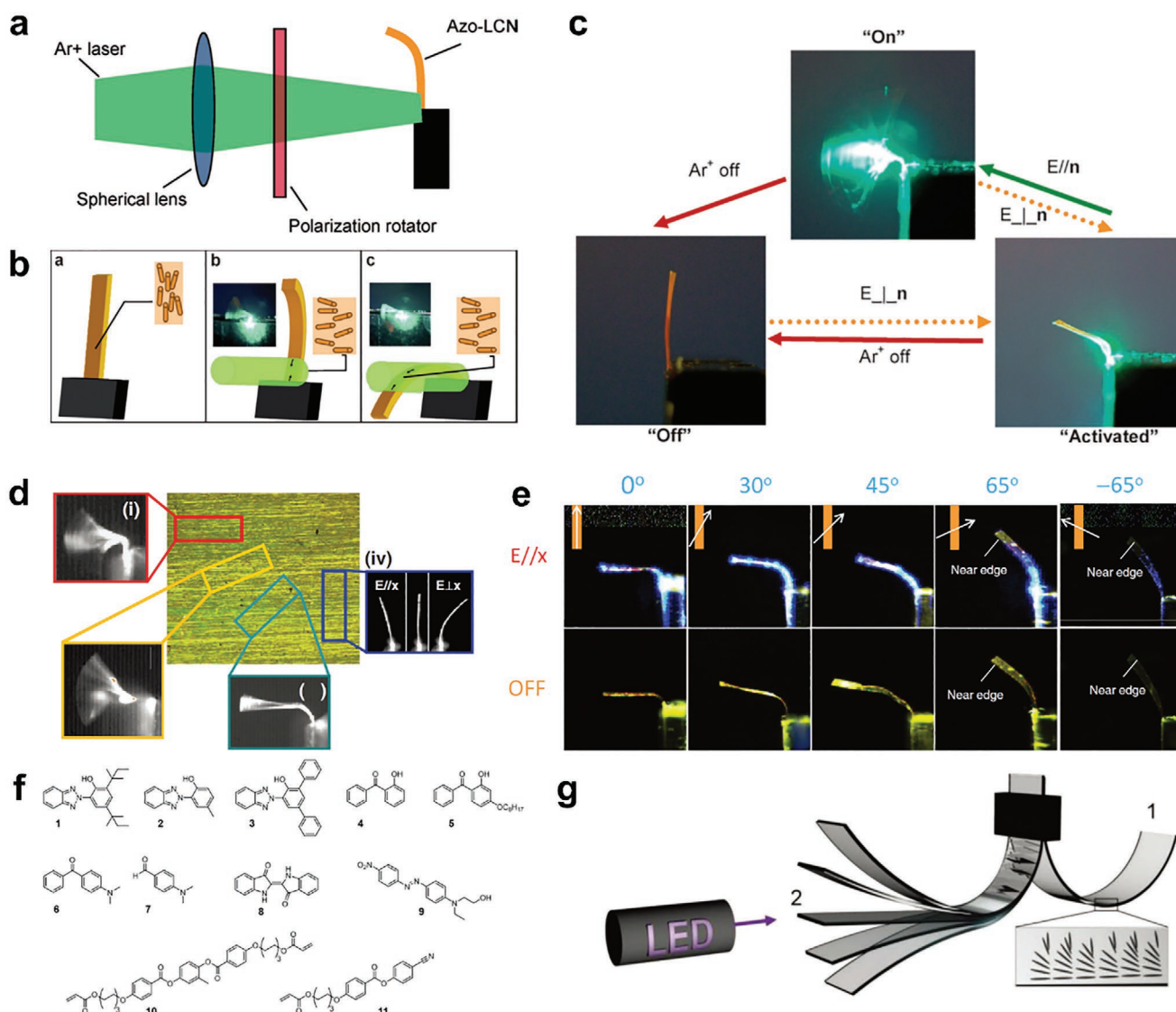
Figure 5. a) Schematic showing of the optical setup for the photoactuation of LC cantilever utilizing the multiwavelength output (457, 488, and 514 nm) of an argon-ion (Ar+) laser, a spherical lens, and a polarization rotator. b) The oscillation mechanism of the LC cantilever. c) The optical protocol for turning the LC cantilever oscillation "'on'" and "'off'". Cycling the Ar+ laser from E⊥n to E∥n can turn oscillation "'on'". The oscillation is turned "'off'" by either blocking the Ar+ or returning the polarization of the laser beam to E⊥n. Reproduced with permission.[112] Copyright 2008, Royal Society of Chemistry. d) Polarized optical micrograph (POM) of the LCP film and photomechanical response of each LC cantilever with nematic director cut (i) 0°, (ii) 15°, (iii) 45°, and (iv) 90° to the cantilever long axis (x). e) In plane bending and out of plane twisting observed of LC cantilevers with the nematic director aligned 0°, 30°, 45°, 65°, and −65° to the cantilever long axis (x) when exposed to 200 mW cm−2 (442 nm) polarized parallel to x. Reproduced with permission.[113] Copyright 2011, Wiley-VCH. f) Chemical structures of photostabilizers 1–7 and dyes 8, 9 incorporated in commercially produced reactive mesogens 10, 11 to obtain self-oscillating LCP films by photopolymerization. g). Schematic representation of the setup and the splay alignment (inset). Initially the film is curved (position 1). When the light is switched on, the film bends toward the light (position 2) where it starts oscillating. Reproduced with permission.[114] Copyright 2017, Wiley-VCH.

3.3. Pumps

Compared to motors and oscillators, pumps can not only provide energy output but also transport liquids and gases. For instance, piston pumps can drive the motion of gas and liquid through the reciprocating movement of the piston. Therefore, they can carry and release odor signals on command, which may be useful to construct olfactory feedback for MR applications. To build these pumps by LCPs is expected to be compatible with miniaturized devices, giving additional tools for future MR wearable equipment.

For example, by placing a deformable azo-LCP onto a rubber membrane in a sealed chamber, Yu et al. developed prototypes of photo-controlled micropumps.[80] In this design, the azo-LCP film was at an unconstrained state so that it produced large deformation in response to UV light (150 mW cm−2). As a result, the azo-LCP film was able to bend the rubber pump membrane that owned a Young's modulus of 1.6 MPa, thereby squeezing the liquid from the chamber. Upon visible illumination, the azo-LCP recovered and the rubber membrane bounced back. Hence, by the alternating irradiation of UV and visible light, the pump was able to drive liquid at a flow rate of 6.5 µL min−1.

Besides driving liquid by external force, it is known that liquid can be self-propelled to the narrow end in a conical channel driven by capillary force[116] (**Figure 6**a). Inspired by this, Yu et al. constructed a microtubular actuator with phototunable diameter and realized the liquid manipulation by

photo-induced capillary force (Figure 6b).[117] Through a newly-developed linear azo-LCP (LLCP) with excellent mechanical properties and processability (Figure 6c), they facilely prepared microtubular actuators of various geometries (i.e., serpentine, helical, and Y-shapes, Figure 6d) with good LC orientation by a
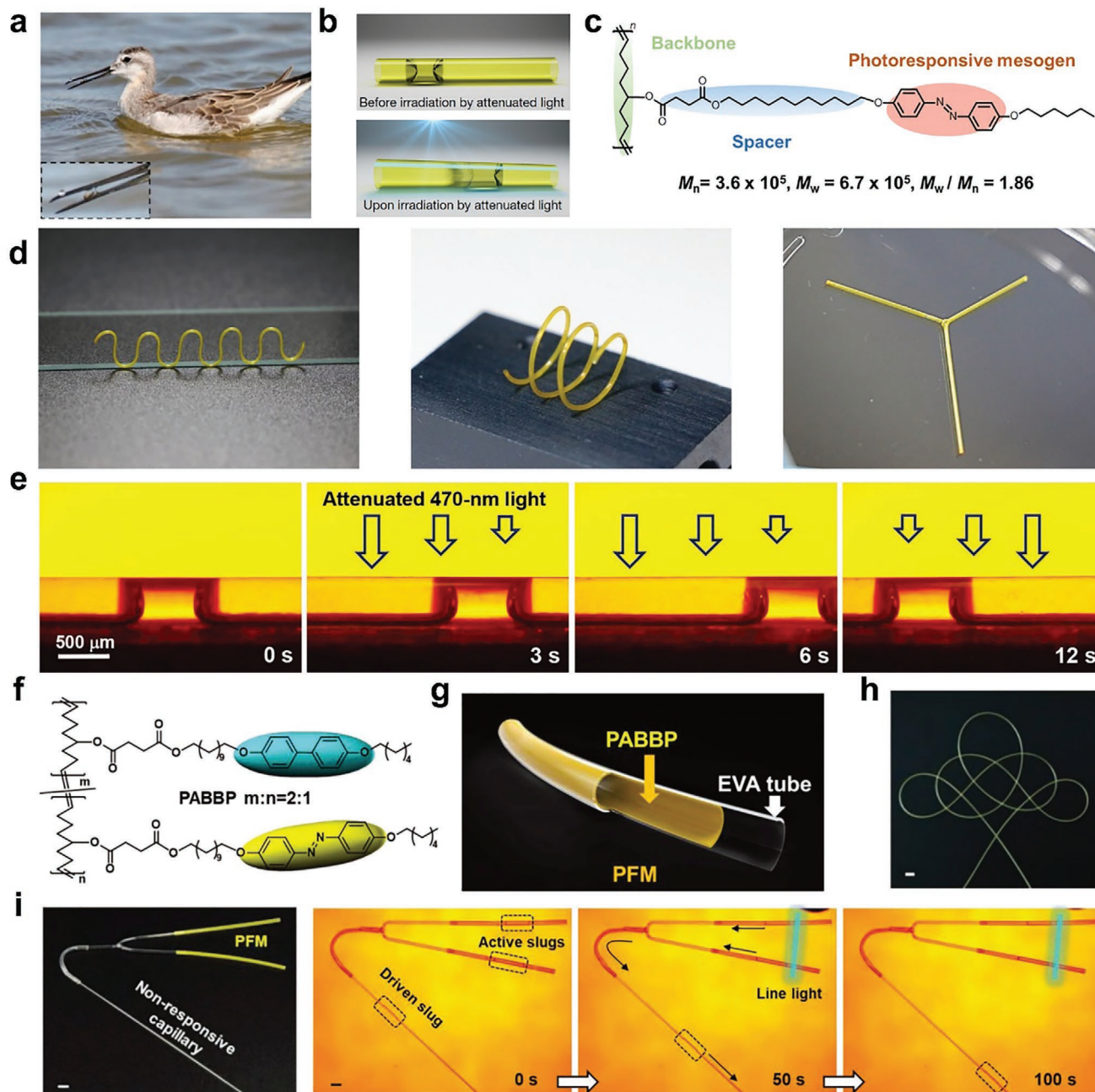
Figure 6. a) Capillary force induced liquid moving to the narrow end of the bird beak during preying. Reproduced with permission.[116] Copyright 2008, American Association for the Advancement of Science. b) Schematics showing the motion of a slug of fully wetting liquid confined in a TMA driven by photodeformation. c) Chemical structure of a novel LLCP. M_n, number average molecular weight; M_w, weight-average molecular weight. d) Images of freestanding serpentine, helical, and Y-shaped microtubular actuators. e) Lateral images of the light-induced motion of a silicone oil slug in a microtubular actuator. Reproduced with permission.[117] Copyright 2016, Springer Nature. f) Chemical structure of the LLCP derivative containing both azobenzene and biphenyl mesogens. g) Schematic representation of PFMs. h) Images of knot actuator fabricated by PFMs. Scale bar, 2 mm. i) Images of a photo-controlled micropump which was composed of two PFMs with a non-responsive microtube. The intensity of the 470 nm line light irradiated on the active slugs was 120 mW cm^{-2}. Scale bar, 5 mm. Reproduced with permission.[118] Copyright 2019, Wiley-VCH.

ADVANCED
SCIENCE NEWS
www.advancedsciencenews.com

ADVANCED
FUNCTIONAL
MATERIALS
www.afm-journal.de

casting, etching, and annealing process. Applying the Weigert effect through an attenuated unpolarized blue light (470 nm, 80 mW cm^{-2}), azobenzene LC mesogens reoriented along the direction of incident light via the continuous *trans–cis–trans* photoisomerization, causing the diameter expansion of LLCP microtubular actuators. As a result, the microtubular actuator formed a cone-like structure, generating asymmetric capillary force to driven the inner liquids (Figure 6e).[116]

By coating a LLCP derivative containing both azobenzene and biphenyl mesogens (PABBP, Figure 6f) into the commercial ethyl vinyl acetate microtube inner wall, the same group then obtained photoresponsive flexible microtubular actuators (PFMs) with a faster photo-driven liquid transport (Figure 6g).[118] Superior to the monolayer microtubular actuators, the bilayer PFMs possess better mechanical property against bending and are compatible for batch preparation (Figure 6h). Thanks to the flexibility of these PFMs, they then assembled two PFMs and a non-responsive microtube by a "Y" shaped glass capillary into a photo-controlled micropump (Figure 6i). Through the light manipulation of the "piston" liquid slugs in the two PFMs, they demonstrated the transport of "cargo" in non-responsive microtube. Since the flexible PFMs remain functional under bending conditions, they have potential in wearable microdevices for MR application.

4. Bio-Inspired LC Robots for Environmental Simulation

Even though the current AR system offers a way to enrich the real world by digital information, it fails to provide haptic interaction using current devices. Incorporating AR technology with bio-inspired robotic system will implant artificial elements with both vision and touch simulation into the real world, creating a MR environment with programmable haptic response. Taking advantage of the stimuli-response of LCPs, LC robots can complete bio-inspired actions without complicated computer programs or power supply systems, which is ideal for providing the required haptic feedback. Here, we will introduce the current progress of bio-inspired LC robots.
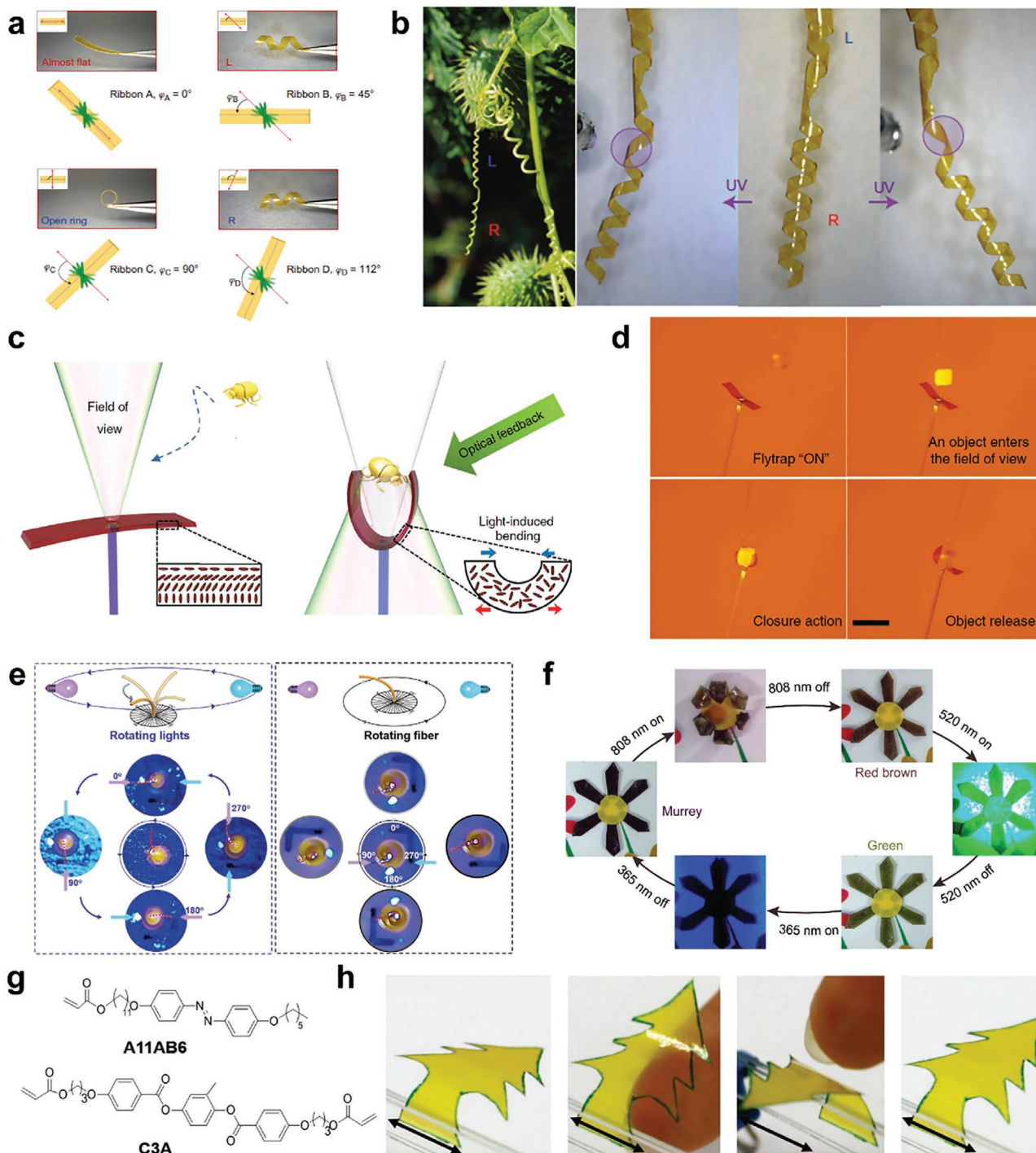
4.1. Artificial Plant LC robots

In nature, certain plants are able to transform environmental stimuli into various mechanical movements. In response to the environmental change, these plants produce molecular signals to trigger the related biological process, leading to complex macroscopic movement. For example, the helical motion of tendril coiling allows the plant to climb up and receive more sunlight for growth. To mimic the performance of tendrils, Katsonis and Fletcher et al. prepared azo-LCP springs exhibiting photo-controlled macroscopic twisting motions.[119] Through the introduction of chiral dopants (S-811 or R-811) in the azo-LCP films, the photoresponsive mesogens were aligned into a left-handed or right-handed twist nematic phase. Therefore, it is possible to obtain ribbons with various LC orientation by simply cutting the films along different directions (**Figure 7**a). As shown in Figure 7b, induced by photoisomerization of azobenzene units,

different deformations including winding, unwinding, and helix inversion were performed from these ribbons under UV irradiation (365 nm, 60 mW cm^{-2}). By selecting suitable chiral films with the aid of light control, the reversible movement and transport of objects were successful. This work displays a facile preparation of smart microactuators, which is useful to assemble MR devices with controllable twisting motions.

The Venus flytrap (*Dionaea muscipula*) can sense the environmental changes, distinguish its prey and react rapidly to adjust its leaves from an open state to a close state within 100 ms. Inspired by its unique property, Zeng and Priimagi et al. created a light-powered LC flytrap, which is composed of a splayed-aligned LCP film doped with Dispersed Red 1 as a gripper and an optical fiber to supply optical feedback.[120] When an object approached, its reflected/scattered light heated up the gripper surface, inducing the LC phase transition. Thus, the gripper was able to bend upward to grasp the object (Figure 7c,d). Due to the different reflective properties among objects, the response threshold of this artificial LC flytrap allowed to distinguish objects made of different materials, which may be useful for item screening. The feedback system in this work provides a new strategy for the active haptic response in MR application.

Heliotropism is a common feature in many plants to receive more sunlight for their growth. By introducing single-walled carbon nanotubes (SWCNTs) into nematic LCP matrix, Jiang et al. have prepared LCP nanocomposite actuators and fabricated them into a "sunflower"-like solar cell device.[121] Served as excellent photothermal agent with good thermal conductivity, SWCNT absorbed the light energy and converted it into thermal energy upon light illumination, heating up the LCP matrix above the nematic-isotropic transition temperature (68 °C). Therefore, the LCP composite actuators facing the sunlight shrunk and tilted the device toward the sun, converting light energy to electrical signals. In 2016, Broer et al. reported a photoresponsive fiber array made of azo-LCPs through a drop-casting and drawing method.[122] Adapting this approach to fabricate photoresponsive fibers, Broer and Schenning et al. then mimic the heliotropism of sunflower and constructed fiber arrays possessing the function of light tracking as well as light guiding.[123] Upon illumination of UV and visible light from opposite direction, these fibers rotated and tracked UV light 360° azimuthally and continuously at ambient temperature (Figure 7e). Meanwhile, the light guiding of these fibers was achieved by placing them onto a red emitting fluorescent dye-doped polymethyl methacrylate (PMMA) plate. By matching the refractive indices between the LCP fibers with PMMA plate, total internal reflection within these LCP fibers was realized. The direction of output light was able to be guided by the bending of these LCP fibers when exposed to UV light, which may be useful for miniaturized optical transport for MR application.

In addition to LC robots that respond to single stimulus, it is foreseeable that these bio-inspired LC robots with multi-response will offer diverse motions and tunable functions to construct more vivid artificial environment. In response to sunlight and internal pH value, some flowers such as Morning Glories and *Hibiscus mutabilis Linn* will bloom and alter their petal color reversibly. To simultaneously mimic the blooming and color change of these flowers, Yang et al. fabricated

**ADVANCED
SCIENCE NEWS**

www.advancedsciencenews.com

**ADVANCED
FUNCTIONAL
MATERIALS**

www.afm-journal.de

Figure 7. a) The ribbons display a variety of shapes that depend on the direction in which they are cutting. b) A coiled tendril of the wild cucumber plant and bionic bending of the spring is achieved and controlled by selective irradiation, which induces a local elongation of the right-handed ribbon. Reproduced with permission.[119] Copyright 2014, Springer Nature. c) Schematic drawing the actuation principle of light-powered LC flytrap. d) The optical flytrap mimics the motion of a natural flytrap by capturing a small scattering object falling on the gripper ($P = 200$ mW). Reproduced with permission.[120] Copyright 2017, Springer Nature. e) Self-regulation of fiber at room temperature in air. The left image shows that fixed fibers continuously adjusted their bending direction to follow the rotation of UV and visible light. The right shows that rotating fibers bent toward the same direction once the position of incident light sources was fixed. Reproduced with permission.[123] Copyright 2020, Wiley-VCH. f) The color changes and blooming/unblooming regulation of tricolor flowers under different mechanisms by light with different wavelengths. Reproduced with permission.[124] Copyright 2018, American Chemical Society g) Chemical structures of the LC monomers used for preparation of the LCP film. h) Images showing the "tree" bending. When a finger is close to the back of "tree," it bends in the direction perpendicular to the LC alignment direction and changes from a back-bend to a forward bends, while it recovers to its original state after the finger is removed. Reproduced with permission.[126] Copyright 2016, Wiley-VCH.

**ADVANCED
SCIENCE NEWS**

www.advancedsciencenews.com

**ADVANCED
FUNCTIONAL
MATERIALS**

www.afm-journal.de

monodomain/polydomain bilayer LCP actuators functionalized by two spiropyran units.[124] Taking advantage of two functionalized spiropyran units with different light response, the color of the LCP actuator was adjustable by varying the wavelength of light stimuli, including UV, green, NIR light (Figure 7f). On the other hand, the LC-isotropic phase transition of LCP upon heating or NIR illumination led to asymmetric contraction of the bilayer structure, producing the controllable bending and unbending, mimicking the blooming of flowers.

Inspired by nocturnal flowers that bloom correlating with both the decrease of light intensity and increase of humidity, Priimagi and Schenning et al. prepared a light and humidity dual responsive LC flower.[125] This LC flower was obtained by copolymerization of an azobenzene derivative (Disperse Red 1 acrylate), a carboxylic acid monomer, and an LC crosslinker. Before the base treatment, the LC flower exhibited reversible blooming and closure at any relative humidity (RH) upon illumination of 450 nm light with an intensity of 100 mW cm^{-2}, which is dominated by LC-isotropic phase transition via photothermal effect. The LC flower after base treatment, however, showed a humidity gated actuation. At low relative humidity (RH), the blooming of LC flower was unsuccessful even upon the illumination of 450 nm light with a high intensity of 100 mW cm^{-2}. When the polymer chains were swollen by moisture at high RH, the decrease the LC order in the LCP was able to be rapidly triggered by a 450 nm light with a lower intensity (8 mW cm^{-2}). By adjusting the initial LC orientation, more complex deformation was achieved by the combined control of light and humidity control.

Instead of using a hydrophilic LC material, Yu et al. realized the humidity and light dual-response from a hydrophobic azo-LCP film. Upon UV illumination (365 nm, 40 mW cm^{-2}), this monodomain nematic azo-LCP film bent toward the light source induced by the photoisomerization of azobenzene units.[126] More interestingly, the film was able to sense a subtle humidity change (i.e., when a finger was approaching) and bent away even though it was hydrophobic with a water contact angle of 91.5°. They attributed this phenomenon by the oxygen-containing functional groups presented in the azo-LCP (Figure 7g). In contact with moisture, hydrogen bond interaction between LC molecules and water molecules disrupted the LC orientation and increased the distance of molecular chain, causing the expansion of the film surface and inducing the bending of the film. Since the response by light and humidity is orthogonal, they assembled a touchless electronic device using this azo-LCP, which is likely to be used as sensors to detect changes in humidity and UV light (Figure 7h).

4.2. Insect-Like LC Robots

There are over 10 million species of insects in the world, which are nearly half of all living species on earth. The different movements of insects have inspired people to develop various soft actuators and robots with complex functions. Introducing bio-inspired LC robots combined with current AR and VR system may not only enrich the artificial environment in MR but also simulate more sensible haptic feedback. For instance, crawling is a basic locomotion of creatures such as worms and
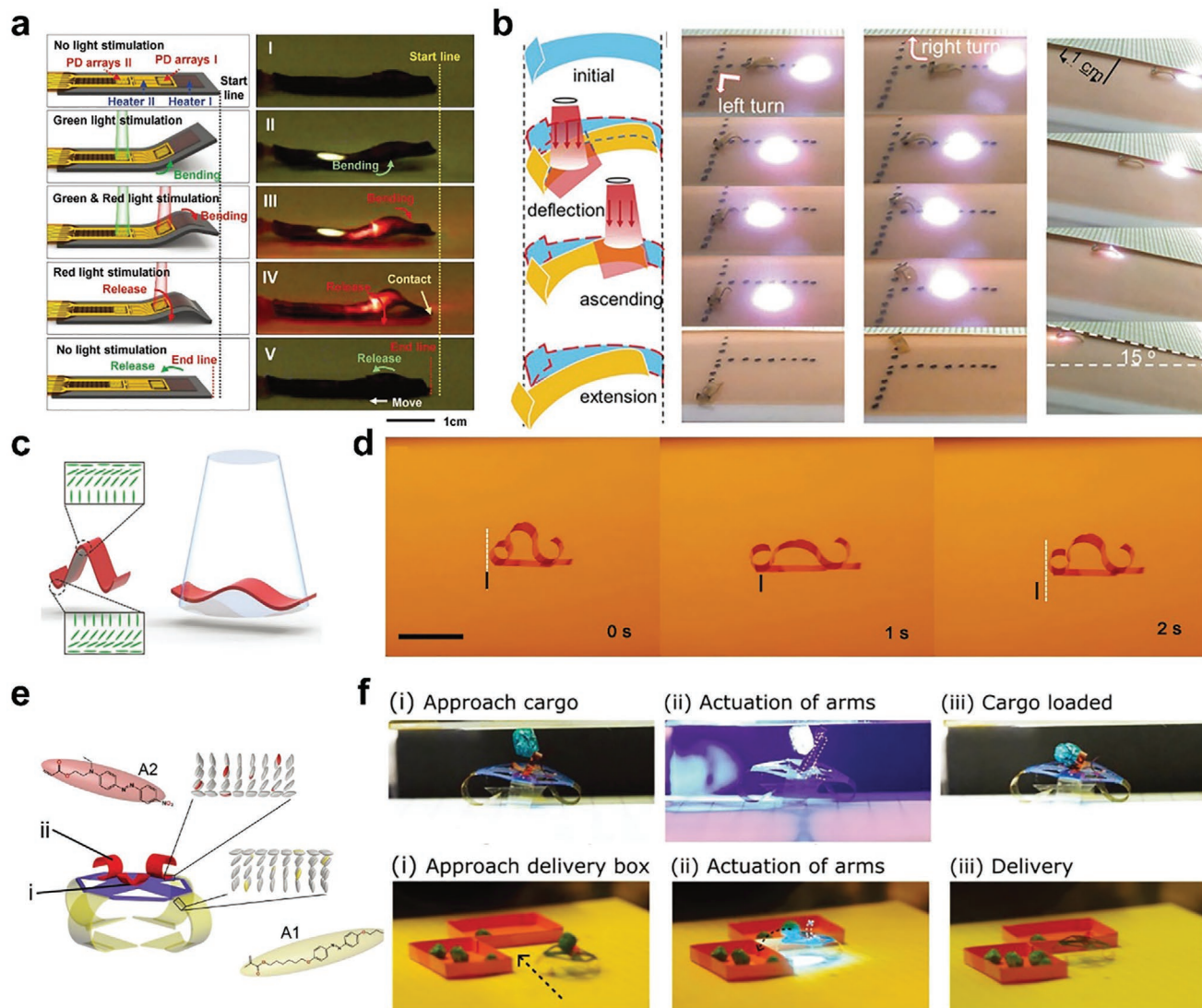
caterpillars. However, current robots are too bulky and rigid so that they are difficult to imitate these simple movements. LC robots, on the contrary, can produce smooth crawling motions in response to stimuli.

Using electricity as a stimulus, Zhao et al. presented bio-inspired "Janus" LC soft robots assembled from electric responsive LC laminate films.[127] The electric responsive LC laminate films were prepared by embedding thin resistance wires between a uniaxially aligned LCP strip and a Kapton layer. Upon Joule heating, this film bent toward the LCP side, while it recovered when cooled, thereby performing a reversible electro-driven actuation. Moreover, this film exhibited an exceptional reprogrammability, which enable it to be reprocessed into desired 2D and 3D structures by simple mechanical and thermal treatment. By assembling these LC laminate films into various "Janus" robots, they demonstrated the bio-inspired loco-motion of these robots on a flat surface as well as in a tube by turning on/off the electric power.

Coupling a stretchable Joule heating component with a thermoresponsive LCP containing carbon black, Yu et al. presented the two-way gait locomotion of an electronically actuated LC robot. The addition of carbon black enhanced the thermal conductivity of LCP as well to improved its structural stability.[128] By controlling the number, distribution, and activation sequences of innervated heaters, more complex and reversible actuation behaviors were realized. Ultrathin Si optoelectronic sensors that respond to light of different wavelength were then introduced to convert it into a photo-controlled LC robot. Upon alternating irradiation of red and green laser beams at different parts, the LC robot performed crawling motion similar to inchworm (**Figure 8**a). It is expected that these LC robots with motion feedback in response to environment will provide better interaction in MR applications.

Compared with electroresponsive LC robots driven by wired cable, photoresponsive LC robots are compatible to remote control, giving a greater freedom to the movement of LC robots. Utilizing photothermal effect, Zhao et al. fabricated a bilayer light-guide LC robot with locomotion of crawling, turning, and twisting by doping a NIR dye, imNi8(4), into a thermoresponsive LCP with one side of crosslinked monodomain (as actuation layer) and the other side of crosslinked polydomain (as non-responsive layer).[129] When laser (980 nm, 3.9 W cm^{-1}) was used to scan the crawling LC robot in different modes, photothermal induced asymmetric contraction allowed the LC robots to perform different movements, that is, moving along a straight line, turning left or right, and climbing an inclined surface (Figure 8b). This work shows advantages of using light as programmable control for microrobot actuation.

To mimic the travelling deformation wave locomotion of caterpillar in a precise manner, Wasylczyk et al. prepared a photothermal-driven crawling LC soft robot made of a patterned LC-orientated thermoresponsive LCP doped with Disperse Orange 3.[130] The photoresponsive LC robot was obtained through polymerizing the LC monomer mixture containing dyes between two glass plates with alternating rubbed/unrubbed stripe patterns. Owing to the patterned LC orientation on the surface, the expansion of LCP only occurred at the LC-aligned domains when was exposed to the laser exposure (532 nm, 480 mW). Thus, the LC robot exhibited travelling

**ADVANCED
SCIENCE NEWS**

www.advancedsciencenews.com

**ADVANCED
FUNCTIONAL
MATERIALS**

www.afm-journal.de

Figure 8. a) The sequential steps of the soft robot to sense and locomote autonomously. The left and right columns are the schematic illustrations and corresponding snap short images. Reproduced with permission.[128] Copyright 2018, Wiley-VCH. b) Laser directed locomotion of a LC robot, including turning left or right, and climbing an inclined surface. Reproduced with permission.[129] Copyright 2018, Wiley-VCH. c) The mesogen alignment in "Ω"-shaped LC robot and deformation mechanisms under the light irradiation: light on → the body extends to a flat structure (i); light off → the body bends to a curved "Ω" structure (ii). d) Inching motion of "Ω" structure soft robot on paper surface. Reproduced with permission.[131] Copyright 2017, Wiley-VCH. e) A schematic depiction of the device, demonstrating the two different light responsive azobenzene chromophores (depicted in yellow and red) used to separately address the legs (yellow) and arms (red) of the cargo handler. f) Cargo loading, transporting, and releasing of LC robot. Reproduced with permission.[132] Copyright 2020, Wiley-VCH.

wave deformation and moved forward when the laser scanned from its tail to head. By switching the intensity and stepping frequency of the laser beam, different action modes were realized to complete various tasks from the LC robot.

To avoid the use of laser beam with high intensity, Priimagi et al. designed a LC soft robot performing crawling locomotion driven by mild visible light. With the aid of patterned alignment layers, an "Ω"-shaped LC robot with patterned splayed orientation was fabricated (Figure 8c).[131] Doped with Disperse Red 1, the LC robot was able to convert light energy into thermal energy, inducing the LC-isotropic phase transition of LCP by visible light at a moderate intensity. Using light as the single

stimulus offered a remote control of this photoresponsive LC robot. Upon a modulated visible (488 nm, 150 mW cm^{-2}, 0.5 Hz) illumination, the LC robot produced reversible deformation between a curved "Ω" structure and a flat structure, moving forward similar to the inching locomotion in caterpillars (Figure 8d).

To enrich crawling LC soft robots with more complex structures and functions, Schenning et al. synthesized a photodriven LC microrobots possessing "arms" and "legs".[132] The legs were prepared by copolymerizing a yellow colored photoswitch A1 with LC monomers to form a photoresponsive LCP with splayed alignment, while the arms were obtained from a

ADVANCED
SCIENCE NEWS
www.advancedsciencenews.com

ADVANCED
FUNCTIONAL
MATERIALS
www.afm-journal.de

splayed oriented LCP containing a red colored photoswitch A2 (Figure 8e). Owing to the difference in absorbance of the two dyes at 455 nm, the actuation of the "arms" with the red dye was more sensitive and with larger amplitude compared to the "legs" with the yellow dye. Hence, by adjusting the intensity of 455 nm light, they managed to control the LC robot via photothermal effect to perform multifunctions including loading, transporting, and releasing cargo (Figure 8f).

4.3. On-Water/Underwater LC Robots

Applying MR technology to provide somatosensory interaction underwater provides a tool for simulating dangerous underwater operations or complex marine environment. Yet, the mimic of underwater scene by current robots and devices is still difficult since these devices require electricity power and with poor water resistance. Moreover, current robots are driven by rigid motors and actuators so that it is challenging to mimic the movement of underwater creatures. LC robots, especially the ones driven by light, are advantageous to act as smart swimming robots. The flexible nature of these robots allows them for various bio-inspired motions such as flagellar motions, giving a more realistic performance.

Cai et al. investigated the NIR light actuation of a soft robot made from a thermoresponsive monodomain LCP coated by polydopamine (PDA).[93] Thanks to the photostability and strong absorption of PDA in the NIR region, it acted as excellent photothermal agent that converted NIR energy into heat, thereby increasing the temperature of the thermoresponsive LCP within one-tenth of a second to induce its rapid contract deformation. By turning NIR light on or off, the LCP composite would bend or unbend accordingly. Thus, this soft robot was able to perform "swimming strokes" at the water–air interface and travelled a distance of 6 mm in 4 s in each NIR irradiation circle.

To avoid the introduction of heat, Yu et al. developed a bilayer-structured light-driven swimmer at liquid/air interfaces, which is composed of an azo-LCP and a commercially available polyimide (Kapton).[133] Triggered by the photochemical phase transition of azo-LCP upon exposure to UV light (150 mW cm^{-2}), the swimmer bent rapid toward the Kapton side within one second. Once the UV light was removed, the swimmer recovered its initial shape in about 2 s. Placed at the liquid/air interface, the swimmer showed a "dolphin kick" motion pattern and moved forward continuous upon UV light at a maximum speed of 1.0 cm s^{-1}.

In addition to the motions at the liquid/air interface, photoresponsive LC robots are able to move and swim underwater. Fischer et al. designed two photoresponsive microrobots made of azo-LCPs with long cylinder and flat disc structures and manipulated their underwater motions by controlling the spatiotemporal distribution and intensity of structured light field using an optical system based on a digital micromirror device (DMD) (**Figure 9**a).[134] The cylindrical LC robot was prepared with axial nematic alignment. Upon UV illumination, it shrunk along the axis while expanded radially owing to the photoisomerization of azobenzene units (Figure 9b). When the cylindrical LC robot was suspended in a solution of glycerol/water

followed by the exposure to a travelling light wave (387 nm, 2 Hz) with a binary periodic pattern of bright and dark stripes, its illuminated part produced local radial expansion and created travelling wave deformations, which drove it to move forward and backward (Figure 9c). On the other hand, the disc-shaped microrobot was obtained with nematic director oriented perpendicular to its surface so that it compressed along the thickness direction while expanded in-plane under the UV exposure. When immersed in silicone oil and exposed to a rotated 2D light pattern, the disc-shape robot exhibited an opposite rotary motion to light at a rate of about 0.5 s^{-1} (Figure 9d). Although the motions in this work remain slow, the combination of closed-loop control software, programmable light pattern and the design of LCPs produces versatile locomotion of LC robots, showing potential in the movement mimic of microorganisms for underwater MR application.

Inspired by the swimming motions of microorganisms, Tian, Yu, Liu and co-workers fabricated a LC swimmer robot that possessed a flexible long flagellum for self-propulsion and a gripper for grabbing and releasing cargo,[135] both of which were driven by azo-LCP films in response to alternating UV light and white light (Figure 9e). Triggered by the photoisomerization of azobenzene units, the azo-LCP film underwent repeating bending and recovery, which induced the wave-like swing of the flexible flagellum, pushing the LC swimmer robot to move toward the target direction. Meanwhile, constructed by a moveable azo-LCP film and a settled polyethylene terephthalate film, the gripper was able to grab, carry, and transport the cargo under the control of light (Figure 9f). Taking advantage from the remote control of light, this microrobot managed to complete different tasks simultaneously or step by step, demonstrating the integration of multi-functional functions into a LC swimmer robot, which may be beneficial to underwater somatosensory interaction in MR.

5. LC Surfaces for Fine Tuning Haptic Response

Surface haptics can output tactile signals to users' bare fingers though the surface deformation of tactile devices. Combining surface haptics with VR/AR will produce MR with versatile tactile feedback to users. Compared with bulky and rigid mechanical components, the use of film-based LCP actuators (LC surfaces) to construct smart tactile devices will greatly reduce their weight and size. In this section, we will brief the recent progress of LC surfaces in surface haptics.

Braille display is one type of tactile devices that are able to deliver tactile information. In 2011, Camargo and coworkers reported a light-controlled Braille display system constructed by a photoresponsive nematic LCP-CNT composite surface with "blisters" pattern.[136] Upon illumination of 660 nm light with power of 13.5 mW, the exposed area of the LCP surface contracted through the photothermal effect, reducing the height of the "blisters" pattern to conceal the tactile information. Although this LCP-based braille display is conceptual, it shows the power of LCP in surface haptics. Later, Torras et al. applied the deformation of the LCP-CNT composite surface to actuate a 10 × 10 haptic pin array (**Figure 10**a) and assembled a portable Braille device with light-tunable patterns (Figure 10b).[137]
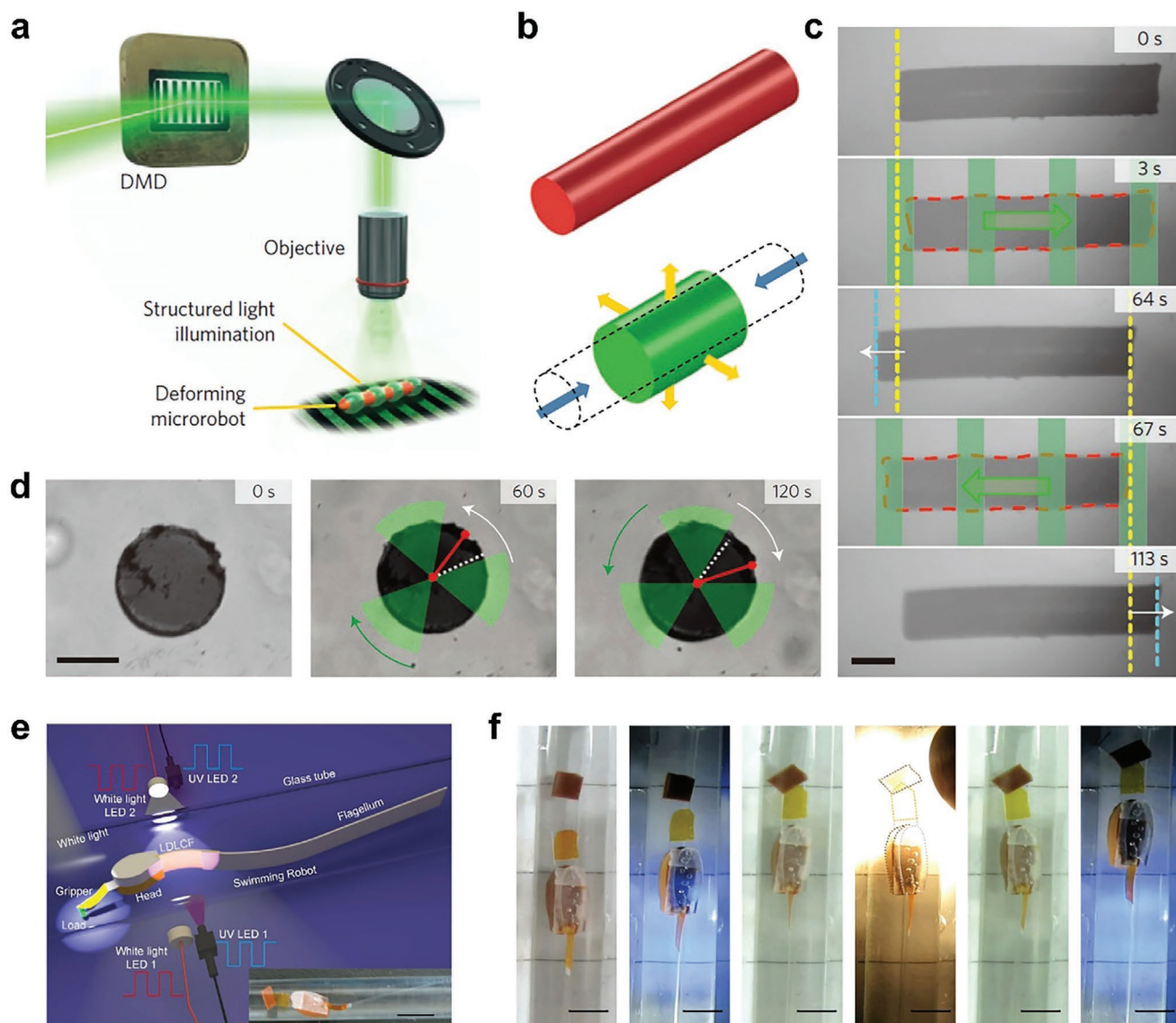
Figure 9. a) The DMD modulates the incoming light beam in both space and time. The microscope objective projects the dynamic light field onto the soft microrobot, which deforms in a selective fashion. b) Finite-element simulation of a cylindrical microrobot (length = 1 mm, diameter = 200 μm) at rest (above) and after full deformation (below). It shrinks along the axis while expands radially owing to the photoisomerization of azobenzene units. c) Back and forth swimming of a cylindrical microrobot propelled by travelling-wave deformations. d) In-place rotation of the same microrobot driven by a rotated 2D light pattern. Reproduced with permission.[134] Copyright 2016, Springer Nature. e) Schematic diagrams of the micro swimming robot and light irradiation system. f) The LC swimmer robot with gripper grabs, carries, and transports the cargo. Scale bar, 3 mm. Reproduced with permission.[135] Copyright 2015, Springer Nature.

Inspired by this mechanism, some groups have developed responsive domes by LC vitrimers, which can be used for braille haptic.[138–140]

In addition to macroscopic deformation, LC surfaces can also generate microscopic deformation to control their surface properties for tactile response. For example, LC surfaces with various regular patterned orientations have demonstrated their morphology regulation by stimuli including heat, electricity, and light, which have been well summarized in other reviews.[39,66,141] To further improve the topological contract of these responsive surfaces, they may be useful for haptic display in future MR applications.

Recently, LC surfaces with more complex morphologies have been reported with reversible and programmable control. These LC surfaces offer new tools for simulating the texture and roughness of object surfaces, providing more comfortable and delicate tactile performances. For example, by spinning coating followed by photopolymerization of a monomer mixture containing chiral dopant, LC and azobenzene units on a glass substrate, Broer et al. have prepared a chiral nematic LC surface with phototunable morphologies.[142] Since the glass substrate was modified by a homeotropic polyimide orientation layer, the orientation of the helix axes was parallel to the LC surface. Although the original LC surface exhibited a minor
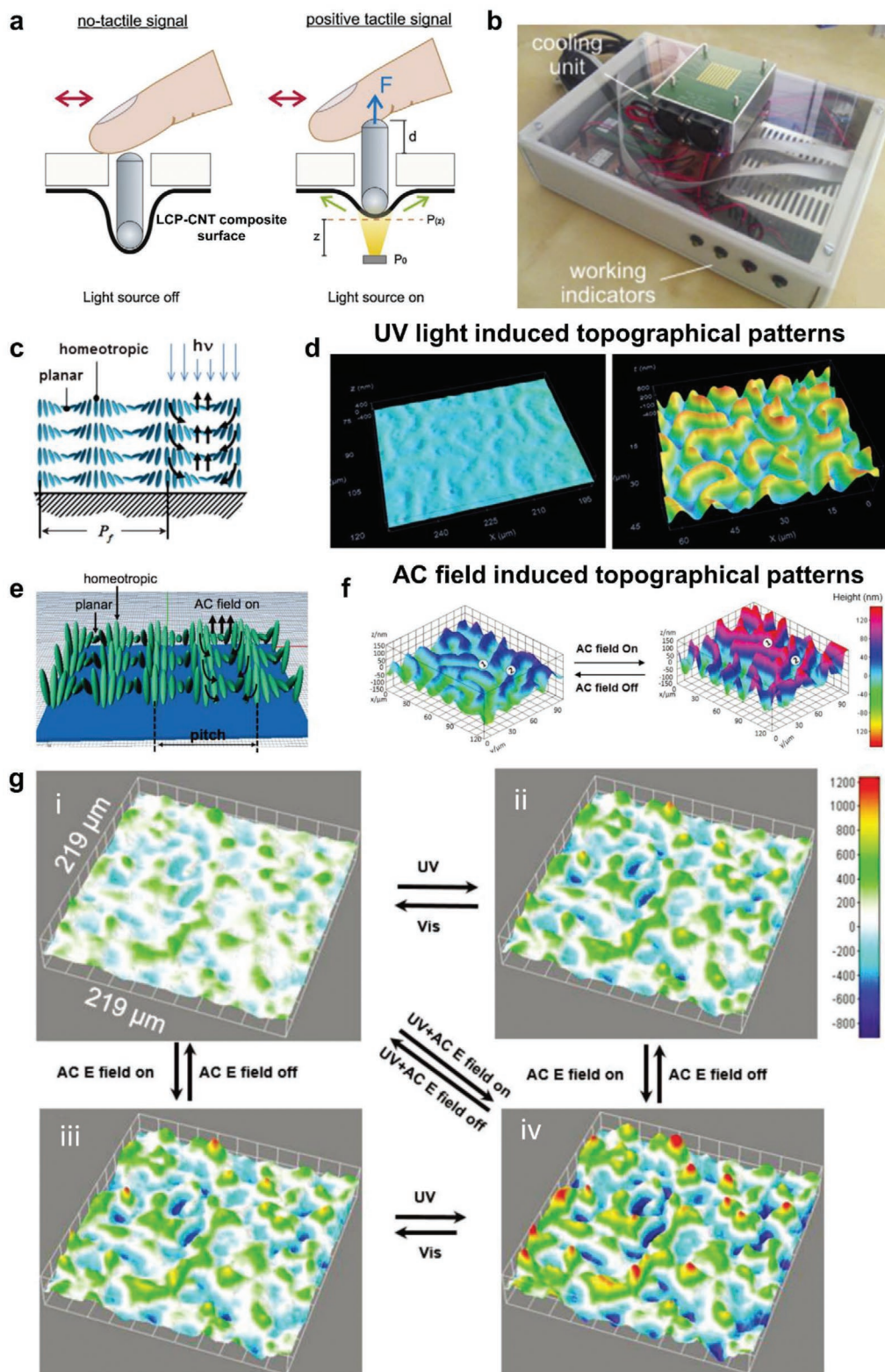
Figure 10. a) Schematic illustrating the actuation of micropins in Braille display controlled by a photoresponsive LCP-CNT composite surface. When the light source is switched off, the LCP-CNT composite surface is in a rest position so that the braille display shows no tactile signal. Upon illumination, the system generates a positive tactile signal with a transmission force F. b) General view of the fully assembled prototype of Braille display with a resolution of 10×10. Reproduced with permission.[137] Copyright 2014, Elsevier. c) Schematic representation of the dynamics of the "fingerprint" texture upon illumination. d) 3D images of the initial flat state and surface topographies under UV exposure. Reproduced with permission.[142] Copyright 2014,

relief under 50 nm owing to the Marangoni effect, it showed a 3D "fingerprint" texture when it was exposed to UV light. Triggered by the *trans–cis* photoisomerization of azobenzene units, protrusions were formed at the points of planar anchoring and wells appeared at the homeotropic positions (Figure 10c). As the photoisomerization of azobenzene units is reversible, the topographical patterns of the LC surface can be switched "on" and "off" repeatedly by light and the height difference of the "fingerprint" texture is adjustable (up to 0.6 µm) in response to the light intensity (Figure 10d). Interestingly, when "fingerprints" were formed, the strain increased more than 20% while its friction coefficient was 1/4–1/5 of that from the flat LC surface, which may be useful to manipulate the surface friction of abovementioned soft actuators and robots, providing more delicate texture mimic. Adding partially insoluble fluorinated acrylate monomers into a similar system, they have demonstrated a randomly ordered polydomain nematic LC surface through facile fabrication.[143] In this case, the size of LC domains was tunable by adding different amounts of fluorinated monomers so that the LC molecules were aligned only within the region of the domain. As a result, the LC surface formed "fingerprint" like structure with 3D spikes of 0.6 µm height difference and exhibited adjustable friction upon UV irradiation.

In addition to light-control, "fingerprints" that can also be modulated by electricity. By introducing LC monomers with polar end group (cyanogroup), Liu et al. presented an electroresponsive LC surface with "fingerprint" texture that can wipe away dust.[144] Inducing by large positive dipole moment under electric field (Figure 10e), the cyano-containing LC monomers deflected, which offered torque forces to change the order parameter, exerting mechanically coupled forces to the polymer network. Since the realignment of LCP is hindered by the high crosslinking density of polymer network, the microscopic molecular voids and related geometrical deformations generated the "fingerprint" texture. When AC electric field (16.1 V_{rms} µm^{-1} at the frequency of 900 kHz) was applied, the orientation of cyano-containing LC monomers alternated as the electric field change. Height of the "fingerprint" oscillated on the surface, producing a net height variation of surface morphology (Figure 10f).

Moreover, they then prepared a multi-domain nematic LC surfaces that generated topographic changes in control of both UV light and electric field.[145] Under AC electric field (16 V_{rms} µm^{-1} at the frequency of 900 kHz), the change of polar mesogen orientation induced the LC surface undergoing order parameter reduction and anisotropic volume expansions, which appeared as "fingerprint" structures on a macroscopic scale. Under UV light (365 nm, 150 mW cm^{-2}) irradiation, the disorderly arrangement of azobenzene molecules inside the LC surface underwent *trans–cis* isomerization, which caused irregular deformation on the surface. More attractively, the degree

of deformation increased when both light and electricity were applied simultaneously and the topology was able to be erased or kept in a bistable state by removing the two stimuli in different sequence (Figure 10g). This dual-stimulus responsive surface enables more complex morphology control, providing a variety of tactile responses.

6. Conclusion and Outlook

We have summarized the recent work of LC actuators and robots, highlighted their actuation modes controlled by electricity and light, and emphasized their potential as haptic devices in MR applications. Through the delicate design of LCP materials and the programming of stimuli, these LC actuators and robots are expected to be used in smart mechanical outputs, wearable and portable devices, bio-inspired robots and surface haptics, providing a new MR world to users. Although the field is still in its infancy, these LC actuators and robots show advantages over their metal analogues toward MR applications owing to their smart response, flexible fabrics, and the wide selection of external stimuli.

At present, the haptic VR equipment suffers from the signal lag, ranging from seconds to minutes.[146–148] It mainly comes from the tedious signal processing processes. For example, to output a mechanical feedback using current VR devices undergoes the following steps.[149] The device needs to receive the command from the environment/user, converting it into digital signals through the circuit and sending it back to computer processing. The computer will then deliver new digital command back through the circuit, activating the mechanical transmission modules in the VR devices to output of the related mechanical signals. Since LCPs are able to convert external stimulus direct into mechanical output,[33,150,151] the MR devices based on LCPs are possible to realize low latency response. However, the response of most current LC actuators and robots remains slow compared with the processing power of computers. Meanwhile, the mechanical strength of LC actuators and robots is still insufficient. Hence, new LCPs with rapid deformation and high mechanical output are demanded for MR applications.

Integrating each functional component, including computer hardware, motor, and mechanical output units into a small and wearable device is another challenge for today's haptic VR devices with desired performance.[152,153] Owing to the lightweight and comfortable textile of LCPs, they are promising candidates for constructing future wearable MR equipment. Yet, the processing of LCPs remains a barrier to their practical use. Although well-oriented LCP film-based actuators and robots have been facilely prepared with the developing of new LCP materials, such as LLCPs and LC vitrimers,[91,138–140] the structures and functions of most current LC devices remain

---

Wiley-VCH. e) Schematic representation of the molecular order and deformation of "fingerprint" LC surface in response to electric field. f) 3D images showing the surface topographies before and during electric actuation. Position 1 points the planar molecular orientation and position 2 is homeotropic orientation. Reproduced with permission.[144] Copyright 2018, Wiley-VCH. g) UV light and electric field orthogonally and synergistically actuated surface topographies. 3D images showing the surface topography of the initial state at RT (i), during UV illumination (ii), under an AC electric field (iii) (16 Vrms µm^{-1}, 900 kHz), and the combined UV illumination and AC field actuation (iv). Reproduced with permission.[145] Copyright 2020, American Chemical Society.

simple due to the limited LC orientation techniques. Hence, the continuous development of new fabrication techniques (i.e., 3D printing[154,51] and excited excimer laser processing[155]) is important for acquiring LC actuators and robots with complex structures, high integration, and multi-functions toward future MR applications.

Replacing wired control with wireless control is a trend to provide better user experience in current VR/AR systems. Therefore, the wireless control of LC actuators and robots will benefit future MR equipment as well. Compared with electricity, light provides non-contact and localized control, which is advantageous in controlling more complex functions of LC actuators and robots. However, the programming and control of the light source will be much more difficult than the electronic control. To avoid interference from ambient light, the control system requires to fine-tune both wavelength and intensity of the stimulating light during operation, which may rely on new computer algorithms and optical sensors. On the other hand, the complex control systems will also new opportunity for MR application. If these LC actuators and robots are able to distinguish computer-programmed light from natural light with the aid of the control system, they may respond to more subtle variation from environment and users, offering a more vivid and real-time MR interaction among human, computers, and environment.

Conflict of Interest

The authors declare no conflict of interest.

[1] S. Feiner, B. Macintyre, D. Seligmann, *Commun. ACM* **1993**, *36*, 53.
[2] R. Azuma, *Commun. ACM* **1993**, *36*, 50.
[3] C. Cruzneira, D. J. Sandin, T. A. Defanti, R. V. Kenyon, J. C. Hart, *Commun. ACM* **1992**, *35*, 64.
[4] J. Carmigniani, B. Furht, M. Anisetti, P. Ceravolo, E. Damiani, M. Ivkovic, *Multimedia Tools Appl.* **2011**, *51*, 341.
[5] H. Kim, Y. T. Kwon, H. R. Lim, J. H. Kim, Y. S. Kim, W. H. Yeo, *Adv. Funct. Mater.* **2020**, *20*, 2005692.
[6] A. K. Yetisen, J. L. Martinez-Hurtado, B. Unal, A. Khademhosseini, H. Butt, *Adv. Mater.* **2018**, *30*, 1706910.
[7] A. M. Sabatini, *Sensors* **2011**, *11*, 1489.
[8] M. Yeh, C. D. Wickens, *Hum. Factors* **2001**, *43*, 355.
[9] S. A. Green, M. Billinghurst, X. Chen, J. G. Chase, *Int. J. Adv. Rob. Syst.* **2008**, *5*, 1.
[10] H. Wu, S. W. Y. Lee, H. Chang, J. Liang, *Comput. Educ.* **2013**, *62*, 41.
[11] C. Cao, R. J. Cerfolio, *Thorac. Surg. Clin.* **2019**, *29*, 329.
[12] Y. C. Fan, C. Y. Wen, *Sensors* **2019**, *19*, 451.
[13] Y. Wang, W. Liu, X. Meng, H. Fu, D. Zhang, Y. Kang, R. Feng, Z. Wei, X. Zhu, G. Jiang, *Appl. Opt.* **2016**, *55*, 6969.
[14] J. Sutherland, J. Belec, A. Sheikh, L. Chepelev, W. Althobaity, B. J. W. Chow, D. Mitsouras, A. Christensen, F. J. Rybicki, D. J. La Russa, *J. Digital Imaging* **2019**, *32*, 38.
[15] D. A. Guttentag, *Tourism Manage.* **2010**, *31*, 637.
[16] S. Aromaa, A. Vaatanen, I. Aaltonen, V. Goriachev, K. Helin, J. Karjalainen, *Appl. Ergon.* **2020**, *88*, 103145.
[17] P. Milgram, F. Kishino, *IEICE Trans. Inf. Syst.* **1994**, *E77D*, 1321.
[18] Z. Pan, A. D. Cheok, H. Yang, J. Zhu, J. Shi, *Comput. Graph.* **2006**, *30*, 20.
[19] A. Y. C. Nee, S. K. Ong, G. Chryssolouris, D. Mourtzis, *CIRP Ann.* **2012**, *61*, 657.
[20] A. Lele, *J. Ambient Intell. Humaniz. Comput.* **2013**, *4*, 17.
[21] H. Hu, X. Feng, Z. Shao, M. Xie, S. Xu, X. Wu, Z. Ye, *Curr. Med. Sci.* **2019**, *39*, 1.
[22] Z. Makhataeva, H. A. Varol, *Robotics* **2020**, *9*, 21.
[23] S. Li, T. Peng, J. Wang, C. Xu, *Chin. J. Mech. Eng.* **2009**, *22*, 403.
[24] J. Kang, *Wireless Pers. Commun.* **2018**, *98*, 1931.
[25] K. Song, S. H. Kim, S. K. S.Jin, S. Lee, J. S. Kim, J. M. Park, Y. Cha, *Sci. Rep.* **2019**, *9*, 8988.
[26] M. A. C. Stuart, W. T. S. Huck, J. Genzer, M. Muller, C. Ober, M. Stamm, G. B. Sukhorukov, I. Szleifer, V. V. Tsukruk, M. Urban, F. Winnik, S. Zauscher, I. Luzinov, S. Minko, *Nat. Mater.* **2010**, *9*, 101.
[27] D. Roy, J. N. Cambre, B. S. Sumerlin, *Prog. Polym. Sci.* **2010**, *35*, 278.
[28] M. Vallet-Regi, F. Balas, D. Arcos, *Angew. Chem., Int. Ed.* **2007**, *46*, 7548.
[29] C. D. H. Alarcon, S. Pennadam, C. Alexander, *Chem. Soc. Rev.* **2005**, *34*, 276.
[30] M. Wei, Y. Gao, X. Li, M. J. Serpe, *Polym. Chem.* **2017**, *8*, 127.
[31] C. Noël, P. Navard, *Prog. Polym. Sci.* **1991**, *16*, 55.
[32] D. Ndaya, R. Bosire, S. Vaidya, R. M. Kasi, *Polym. Chem.* **2020**, *11*, 5937.
[33] T. J. White, D. J. Broer, *Nat. Mater.* **2015**, *14*, 1087.
[34] M. Li, P. Keller, B. Li, X. Wang, M. Brunet, *Adv. Mater.* **2003**, *15*, 569.
[35] H. Finkelmann, E. Nishikawa, G. G. Pereira, M. Warner, *Phys. Rev. Lett.* **2001**, *87*, 015501.
[36] P. G. deGennes, *C. R. Acad. Sci., Ser. IIb: Mec., Phys., Chim., Astron.* **1997**, *324*, 343.
[37] L. T. de Haan, C. Sanchez-Somolinos, C. M. W. Bastiaansen, A. Schenning, D. J. Broer, *Angew. Chem., Int. Ed.* **2012**, *51*, 12469.
[38] S. K. Ahn, T. H. Ware, K. M. Lee, V. P. Tondiglia, T. J. White, *Adv. Funct. Mater.* **2016**, *26*, 5819.
[39] M. E. McConney, A. Martinez, V. P. Tondiglia, K. M. Lee, D. Langley, I. I. Smalyukh, T. J. White, *Adv. Mater.* **2013**, *25*, 5880.
[40] T. Ikeda, M. Nakano, Y. Yu, O. Tsutsumi, A. Kanazawa, *Adv. Mater.* **2003**, *15*, 201.
[41] Y. Yu, M. Nakano, T. Ikeda, *Nature* **2003**, *425*, 145.
[42] T. Ikeda, J. Mamiya, Y. Yu, *Angew. Chem., Int. Ed.* **2007**, *46*, 506.
[43] S. Iamsaard, E. Anger, S. J. Asshoff, A. Depauw, S. P. Fletcher, N. Katsonis, *Angew. Chem., Int. Ed.* **2016**, *55*, 9908.
[44] J. J. Wie, M. R. Shankar, T. J. White, *Nat. Commun.* **2016**, *7*, 13260.
[45] M. Wang, B. Lin, H. Yang, *Nat. Commun.* **2016**, *7*, 13981.
[46] X. Qing, L. Qin, W. Gu, Y. Yu, *Liq. Cryst.* **2016**, *43*, 2114.

[47] L. T. de Haan, J. M. N. Verjans, D. J. Broer, C. W. M. Bastiaansen, A. Schenning, *J. Am. Chem. Soc.* **2014**, *136*, 10585.

[48] W. Wu, L. Yao, T. Yang, R. Yin, F. Li, Y. Yu, *J. Am. Chem. Soc.* **2011**, *133*, 15810.

[49] Y. Ide, Z. Ophir, *Polym. Eng. Sci.* **1983**, *23*, 261.

[50] X. Pang, J. Lv, C. Zhu, L. Qin, Y. Yu, *Adv. Mater.* **2019**, *31*, 1904224.

[51] A. Kotikian, R. L. Truby, J. W. Boley, T. J. White, J. A. Lewis, *Adv. Mater.* **2018**, *30*, 1706164.

[52] M. Lopez-Valdeolivas, D. Liu, D. J. Broer, C. Sanchez-Somolinos, *Macromol. Rapid Commun.* **2018**, *39*, 1700710.

[53] H. Zeng, P. Wasylczyk, D. S. Wiersma, A. Priimagi, *Adv. Mater.* **2018**, *30*, 1703554.

[54] X. Lu, H. Zhang, G. Fei, B. Yu, X. Tong, H. Xia, Y. Zhao, *Adv. Mater.* **2018**, *30*, 1706597.

[55] M. O. Saed, C. P. Ambulo, H. Kim, R. De, V. Raval, K. Searles, D. A. Siddiqui, J. M. O. Cue, M. C. Stefan, M. R. Shankar, T. H. Ware, *Adv. Funct. Mater.* **2019**, *29*, 1806412.

[56] Y. Kim, H. Yuk, R. Zhao, S. A. Chester, X. Zhao, *Nature* **2018**, *558*, 274.

[57] X. Qian, Q. Chen, Y. Yang, Y. Xu, Z. Li, Z. Wang, Y. Wu, Y. Wei, Y. Ji, *Adv. Mater.* **2018**, *30*, 1801103.

[58] X. Kuang, D. J. Roach, J. Wu, C. M. Hamel, Z. Ding, T. Wang, M. L. Dunn, H. Qi, *Adv. Funct. Mater.* **2019**, *29*, 1805290.

[59] M. P. da Cunha, M. G. Debije, A. P. H. J. Schenning, *Chem. Soc. Rev.* **2020**, *49*, 6568.

[60] J. Liu, Y. Gao, Y. J. Lee, S. Yang, *Trends Chem.* **2020**, *2*, 107.

[61] T. Matsushima, K. Seki, S. Kimura, T. Iwakabe, T. Yata, Y. Watanabe, S. Komura, *J. Soc. Inf. Disp.* **2018**, *26*, 602.

[62] J. R. Talukder, Y. Huang, S. Wu, *Liq. Cryst.* **2019**, *46*, 920.

[63] F. Gou, H. Chen, M. Li, S. Lee, S. Wu, *Opt. Express* **2017**, *25*, 7984.

[64] S. Mayr, M. Kopper, A. Buchner, *Displays* **2017**, *48*, 41.

[65] K. Aksit, J. Kautz, D. Luebke, *Appl. Opt.* **2015**, *54*, 3422.

[66] C. Zhu, Y. Lu, J. Sun, Y. Yu, *Langmuir* **2020**, *36*, 6611.

[67] T. J. White, *J. Polym. Sci., Part B: Polym. Phys.* **2018**, *56*, 695.

[68] Y. Shang, J. Wang, T. Ikeda, L. Jiang, *J. Mater. Chem. C* **2019**, *7*, 3413.

[69] C. Yuan, D. J. Roach, C. K. Dunn, Q. Mu, X. Kuang, C. M. Yakacki, T. Wang, K. Yu, H. Qi, *Soft Matter* **2017**, *13*, 5558.

[70] T. H. Ware, T. J. White, *Polym. Chem.* **2015**, *6*, 4835.

[71] Z. Jiang, Y. Xiao, Y. Zhao, *Adv. Opt. Mater.* **2019**, *7*, 1900262.

[72] Z. S. Davidson, H. Shahsavan, A. Aghakhani, Y. Guo, L. Hines, Y. Xia, S. Yang, M. Sitti, *Sci. Adv.* **2019**, *5*, eaay0855.

[73] R. Williams, *J. Chem. Phys.* **1963**, *39*, 384.

[74] S. Tazuke, S. Kurihara, H. Yamaguchi, T. Ikeda, *J. Phys. Chem.* **1987**, *91*, 249.

[75] W. Lehmann, H. Skupin, C. Tolksdorf, E. Gebhard, R. Zentel, P. Kruger, M. Losche, F. Kremer, *Nature* **2001**, *410*, 447.

[76] T. Guin, B. A. Kowalski, R. Rao, A. D. Auguste, C. A. Grabowski, P. F. Lloyd, V. P. Tondiglia, B. Maruyama, R. A. Vaia, T. J. White, *ACS Appl. Mater. Interfaces* **2018**, *10*, 1187.

[77] M. Chambers, H. Finkelmann, M. Remskar, A. Sanchez-Ferrer, B. Zalar, S. Zumer, *J. Mater. Chem.* **2009**, *19*, 1524.

[78] L. Tan, A. C. Davis, D. J. Cappelleri, *Adv. Funct. Mater.* **2020**, 2007125. https://doi.org/10.1002/adfm.202007125

[79] J. Küpfer, H. Finkelmann, *Makromol. Chem., Rapid Commun.* **1991**, *12*, 717.

[80] Q. He, Z. Wang, Y. Wang, A. Minori, M. T. Tolley, S. Q. Cai, *Sci. Adv.* **2019**, *5*, eaax5746.

[81] M. J. Ford, C. P. Ambulo, T. A. Kent, E. J. Markvicka, C. F. Pan, J. Malen, T. H. Ware, C. Majidi, *Proc. Natl. Acad. Sci. USA* **2019**, *116*, 21438.

[82] T. A. Kent, M. J. Ford, E. J. Markvicka, C. Majidi, *Multifunct. Mater.* **2020**, *3*, 025003.

[83] J. Wei, Y. Yu, *Soft Matter* **2012**, *8*, 8050.

[84] Z. Wang, H. Zhang, *Chin. J. Polym. Sci.* **2020**, *38*, 37.

[85] S. Han, Y. Chen, B. Xu, J. Wei, Y. Yu, *Chin. J. Polym. Sci.* **2020**, *38*, 806.

[86] L. Dong, Y. Zhao, *Mater. Chem. Front.* **2018**, *2*, 1932.

[87] M. P. da Cunha, E. A. J. van Thoor, M. G. Debije, D. J. Broer, A. Schenning, *J. Mater. Chem. C* **2019**, *7*, 13502.

[88] L. Liu, M. Liu, L. Deng, B. Lin, H. Yang, *J. Am. Chem. Soc.* **2017**, *139*, 11333.

[89] Y. Wang, A. Dang, Z. Zhang, R. Yin, Y. Gao, L. Feng, S. Yang, *Adv. Mater.* **2020**, *32*, 2004270.

[90] J. E. Marshall, Y. Ji, N. Torras, K. Zinoviev, E. M. Terentjev, *Soft Matter* **2012**, *8*, 1570.

[91] Y. Yang, Z. Pei, Z. Li, Y. Wei, Y. Ji, *J. Am. Chem. Soc.* **2016**, *138*, 2118.

[92] Z. Li, Y. Yang, Z. Wang, X. Zhang, Q. Chen, X. Qian, N. Liu, Y. Wei, Y. Ji, *J. Mater. Chem. A* **2017**, *5*, 6740.

[93] H. Tian, Z. Wang, Y. Chen, J. Shao, T. Gao, S. Cai, *ACS Appl. Mater. Interfaces* **2018**, *10*, 8307.

[94] T. Ube, T. Ikeda, *Adv. Opt. Mater.* **2019**, *7*, 1900380.

[95] A. S. Kuenstler, Y. Chen, P. Bui, H. Kim, A. DeSimone, L. Jin, R. C. Hayward, *Adv. Mater.* **2020**, *32*, 2000609.

[96] Y. Ishibashi, S. Nakai, K. Masuda, D. Kitagawa, S. Kobatake, T. Asahi, *Chem. Commun.* **2020**, *56*, 7088.

[97] M. Lahikainen, K. Kuntze, H. Zeng, S. Helantera, S. Hecht, A. Priimagi, *ACS Appl. Mater. Interfaces* **2020**, *12*, 47939.

[98] M. J. Moran, M. Magrini, D. M. Walba, I. Aprahamian, *J. Am. Chem. Soc.* **2018**, *140*, 13623.

[99] G. Vantomme, A. H. Gelebart, D. J. Broer, E. W. Meijer, *Tetrahedron* **2017**, *73*, 4963.

[100] X. M. Mu, N. Sowan, J. A. Tumbic, C. N. Bowman, P. T. Mather, H. J. Qi, *Soft Matter* **2015**, *11*, 2673.

[101] K. M. Lee, T. J. White, *Macromolecules* **2012**, *45*, 7163.

[102] F. Cheng, R. Yin, Y. Zhang, C. Yen, Y. Yu, *Soft Matter* **2010**, *6*, 3447.

[103] F. Weigert, *Verh. Dtsch. Phys. Ges.* **1919**, *21*, 479.

[104] T. Ube, T. Ikeda, *Angew. Chem., Int. Ed.* **2014**, *53*, 10290.

[105] X. Qing, J. Lv, Y. Yu, *Acta Polym. Sin.* **2017**, *11*, 1679.

[106] K. M. Lee, N. V. Tabiryan, T. J. Bunning, T. J. White, *J. Mater. Chem.* **2012**, *22*, 691.

[107] M. Yamada, M. Kondo, J. I. Mamiya, Y. Yu, M. Kinoshita, C. J. Barrett, T. Ikeda, *Angew. Chem., Int. Ed.* **2008**, *47*, 4986.

[108] M. Wang, Z. Cheng, B. Zuo, X. Chen, S. Huang, H. Yang, *ACS Macro Lett.* **2020**, *9*, 860.

[109] C. Ahn, K. Li, S. Cai, *ACS Appl. Mater. Interfaces* **2018**, *10*, 25689.

[110] K. Dradrach, M. Rogoz, P. Grabowski, C. Xuan, R. Weglowski, J. Konieczkowska, E. Schab-Balcerzak, W. Piecek, P. Wasylczyk, *ACS Appl. Mater. Interfaces* **2020**, *12*, 8681.

[111] K. Y. Ma, P. Chirarattananon, S. B. Fuller, R. J. Wood, *Science* **2013**, *340*, 603.

[112] T. J. White, N. V. Tabiryan, S. V. Serak, U. A. Hrozhyk, V. P. Tondiglia, H. Koerner, R. A. Vaia, T. J. Bunning, *Soft Matter* **2008**, *4*, 1796.

[113] S. Serak, N. Tabiryan, R. Vergara, T. J. White, R. A. Vaia, T. J. Bunning, *Soft Matter* **2010**, *6*, 779.

[114] K. M. Lee, M. L. Smith, H. Koerner, N. Tabiryan, R. A. Vaia, T. J. Bunning, T. J. White, *Adv. Funct. Mater.* **2011**, *21*, 2913.

[115] A. H. Gelebart, G. Vantomme, E. W. Meijer, D. J. Broer, *Adv. Mater.* **2017**, *29*, 1606712.

[116] M. Prakash, D. Quere, J. W. M. Bush, *Science* **2008**, *320*, 931.

[117] J. Lv, Y. Liu, J. Wei, E. Chen, L. Qin, Y. Yu, *Nature* **2016**, *537*, 179.

[118] B. Xu, C. Zhu, L. Qin, J. Wei, Y. Yu, *Small* **2019**, *15*, 1901847.

[119] S. Iamsaard, S. J. Asshoff, B. Matt, T. Kudernac, J. Cornelissen, S. P. Fletcher, N. Katsonis, *Nat. Chem.* **2014**, *6*, 229.

[120] O. M. Wani, H. Zeng, A. Priimagi, *Nat. Commun.* **2017**, *8*, 15546.

[121] C. Li, Y. Liu, X. Huang, H. Jiang, *Adv. Funct. Mater.* **2012**, *22*, 5166.

[122] A. H. Gelebart, M. Mc Bride, A. Schenning, C. N. Bowman, D. J. Broer, *Adv. Funct. Mater.* **2016**, *26*, 5322.

[123] L. Liu, M. delpozo , F. Mohseninejad, M. G. Debije, D. J. Broer, A. Schenning, *Adv. Opt. Mater.* **2020**, *8*, 2000732.

[124] B. Zuo, M. Wang, B. Lin, H. Yang, *Chem. Mater.* **2018**, *30*, 8079.

[125] O. M. Wani, R. Verpaalen, H. Zeng, A. Priimagi, A. Schenning, *Adv. Mater.* **2019**, *31*, 1805985.

[126] Y. Liu, B. Xu, S. Sun, J. Wei, L. Wu, Y. Yu, *Adv. Mater.* **2017**, *29*, 1604792.

[127] Y. Xiao, Z. Jiang, X. Tong, Y. Zhao, *Adv. Mater.* **2019**, *31*, 1903452.

[128] C. Wang, K. Sim, J. Chen, H. Kim, Z. Rao, Y. Li, W. Chen, J. Song, R. Verduzco, C. Yu, *Adv. Mater.* **2018**, *30*, 1706695.

[129] F. Ge, R. Yang, X. Tong, F. Camerel, Y. Zhao, *Angew. Chem., Int. Ed.* **2018**, *57*, 11758.

[130] M. Rogóż, H. Zeng, C. Xuan, D. S. Wiersma, P. Wasylczyk, *Adv. Opt. Mater.* **2016**, *4*, 1689.

[131] H. Zeng, O. M. Wani, P. Wasylczyk, A. Priimagi, *Macromol. Rapid Commun.* **2018**, *39*, 1700224.

[132] M. Pilz da Cunha, S. Ambergen, M. G. Debije, E. Homburg, J. M. J. den Toonder, A. , Schenning, *Adv. Sci.* **2020**, *7*, 1902842.

[133] S. Ma, X. Li, S. Huang, J. Hu, H. Yu, *Angew. Chem., Int. Ed.* **2019**, *58*, 2655.

[134] S. Palagi, A. G. Mark, S. Y. Reigh, K. Melde, T. Qiu, H. Zeng, C. Parmeggiani, D. Martella, A. Sanchez-Castillo, N. Kapernaum, F. Giesselmann, D. S. Wiersma, E. Lauga, P. Fischer, *Nat. Mater.* **2016**, *15*, 647.

[135] C. Huang, J. Lv, X. Tian, Y. Wang, Y. Yu, J. Liu, *Sci. Rep.* **2015**, *5*, 17414.

[136] C. J. Camargo, N. Torras, H. Campanella, J. E. Marshall, K. Zinoviev, E. M. Campo, E. M. Terentjev, J. Esteve, in *Proceedings of SPIE* (Eds: J. Esteve, E. M. Terentjev, E. M. Campo, 2011, *8107*, p. 810709.

[137] N. Torras, K. E. Zinoviev, C. J. Camargo, E. M. Campo, H. Campanella, J. Esteve, J. E. Marshall, E. M. Terentjev,

M. Omastova, I. Krupa, P. Teplicky, B. Mamojka, P. Bruns, B. Roeder, M. Vallribera, R. Malet, S. Zuffanelli, V. Soler, J. Roig, N. Walker, D. Wenn, F. Vossen, F. M. H. Crompvoets, *Sens. Actuators, A* **2014**, *208*, 104.

[138] M. O. Saed, A. Gablier, E. M. Terentjev, *Adv. Funct. Mater.* **2020**, *30*, 1906458.

[139] Y. Yang, E. M. Terentjev, Y. Zhang, Q. Chen, Y. Zhao, Y. Wei, Y. Ji, *Angew. Chem., Int. Ed.* **2019**, *58*, 17474.

[140] Y. Yang, E. M. Terentjev, Y. Wei, Y. Ji, *Nat. Commun.* **2018**, *9*, 1906.

[141] D. Liu, D. J. Broer, *Liq. Cryst. Rev.* **2013**, *1*, 20.

[142] D. Liu, D. J. Broer, *Angew. Chem., Int. Ed.* **2014**, *53*, 4542.

[143] D. Liu, L. Liu, P. R. Onck, D. J. Broer, *Proc. Natl. Acad. Sci. USA* **2015**, *112*, 3880.

[144] W. Feng, D. J. Broer, D. Liu, *Adv. Mater.* **2018**, *30*, 1704970.

[145] W. Feng, D. J. Broer, D. Liu, *Adv. Funct. Mater.* **2020**, *30*, 1901681.

[146] M. S. Elbamby, C. Perfecto, M. Bennis, K. Doppler, *IEEE Network* **2018**, *32*, 78.

[147] K. S. Kim, D. K. Kim, C. B. Chae, S. Choi, Y. C. Ko, J. Kim, Y. G. Lim, M. Yang, S. Kim, B. Lim, K. Lee, K. L. Ryu, *Proc. IEEE* **2019**, *107*, 376.

[148] C. Basdogan, F. Giraud, V. Levesque, S. Choi, *IEEE Trans. Haptics* **2020**, *13*, 450.

[149] N. E. Seymour, J. S. Rotnes, *Surg. Endosc.* **2006**, *20*, 1774.

[150] C. Ohm, M. Brehmer, R. Zentel, *Adv. Mater.* **2010**, *22*, 3366.

[151] H. Zeng, P. Wasylczyk, D. S. Wiersma, A. Prrimagi, *Adv. Mater.* **2018**, *30*, 1703554.

[152] T. Yang, D. Xie, Z. Li, H. Zhu, *Mater. Sci. Eng., R* **2017**, *115*, 1.

[153] J. Shi, S. Liu, L. Zhang, B. Yang, L. Shu, Y. Yang, M. Ren, Y. Wang, J. Chen, W. Chen, *Adv. Mater.* **2019**, *32*, 1901958.

[154] S. Gantenbein, K. Masania, W. Woigk, J. P. W. Sesseg, T. A. Tervoort, A. R. Studart, *Nature* **2018**, *561*, 226.

[155] H. Niino, A. Yabe, *Appl. Phys. Lett.* **1993**, *63*, 3527.

Chongyu Zhu is currently working as an assistant professor in the Department of Materials Science at Fudan University, China. He completed his B.Sc. in the Department of Chemistry, Tsinghua University, China and his Ph.D. in the Department of Chemistry, University of Warwick, U.K. Before joining Fudan University, he worked as a postdoctoral researcher in the Department of Materials Science and Engineering at the University of California, Berkeley, United States. He is currently working on the development of responsive polymer materials for biosensors and medical devices.

Yao Lu is currently a Ph.D. student at the Department of Materials Science, Fudan University (China). He received his B.S. degree in the College of Material Science and Technology at Nanjing University of Aeronautics and Astronautics (China) in 2014. His research interests focus on the construction of liquid crystal polymer soft actuators and the applications in microfluidic.

Yanlei Yu is a professor in the Department of Materials Science at Fudan University, China. She graduated in applied chemistry from Anhui University in 1993 and obtained her M.S. degree in polymer chemistry and physics from the University of Science and Technology of China in 1996. She gained her Ph.D. degree in environmental chemistry and engineering from Tokyo Institute of Technology and was promoted to Full Professor at Fudan University in 2004. Her research interests focus on the development of photodeformable smart materials and light-controllable interface materials with photosensitive polymers and liquid crystal polymers.